Simultaneously assimilating multivariate datasets into the two-source evapotranspiration model by Bayesian approach: Application to spring maize in an arid region of northwest China

G.F. Zhu[1], X. Li [2], Y.H. Su[2], K. Zhang[1], Y. Bai[1], J.Z. Ma[1], C. B. Li[1], X. L. Hu[2], J. H. He[1]

1. Key Laboratory of Western China's Environmental Systems (Ministry of Education), Lanzhou University, Lanzhou 730000, China.
2. Cold and Arid Regions Environmental and Engineering Research Institute, Chinese Academy of Science, Lanzhou 730000, China.

Corresponding Author: Zhu Gaofeng

Address: Tianshui Road 222, Lanzhou, Gnasu Province, China, 730000.

Email: zhugf@lzu.edu.cn

Abstract

Based on direct measurements of half-hourly canopy evapotranspiration (ET; W m^{-2}) using the eddy covariance (EC) system and daily soil evaporation (E; mm d^{-1}) using microlysimeters over a crop ecosystem in arid northwest China from 27 May to 14 Sep. in 2013, a Bayesian method was used to simultaneously parameterize the soil surface and canopy resistances in the Shuttleworth-Wallace (S-W) model. 4 of the six parameters showed relatively larger uncertainty reductions (>50%), and their posterior distributions became approximately symmetric with distinctive modes. There was a moderately good agreement between measured and simulated values of half-hourly ET and daily E with a linear regression being y=0.84x+0.18 (R^2=0.83) and y=1.01x+0.01 (R^2=0.82), respectively. The causes of underestimations of ET by the S-W model was possibly attributed to the micro-scale advection, which can contribute an added energy in the form of downward sensible heat fluxes to the ET process. Therefore, the advection process should be taken into account in simulating ET in heterogeneous land surface. Also, underestimations were observed on or shortly after rainy days, which may be due to direct evaporation of liquid water intercepted in the canopy. Thus, the canopy interception model should be coupled to the S-W model in the long-term ET simulation.

Keywords: Bayesian statistics, Crop evapotranspiration, Shuttleworth-Wallace model, Maize, Arid region

1 Introduction

In agriculture ecosystem, more than 90% of all water inputs is lost by evapotranspiration (ET) (Morison et al., 2008), which is defined as the sum of water loss by evaporation (*E*) from soil and transpiration (*T*) from plants (Rana and Katerji, 2000). *E* and *T* are influenced by different abiotic and biotic factors (Wang and Yakir, 2000), and the contributions of *E* and *T* to the total ecosystem ET are highly variable in space and time (Ferretti et al., 2003). Thus, accurate measurement or estimation of ET and its components (*E* and *T*) is essential for many applications in agriculture, such as irrigation scheduling, drainage, and yield forecasts (Wallace and Verhoef, 2000; Flumignan et al., 2011; Sun et al., 2012). The Shuttleworth-Wallace model (S-W model) (Shuttleworth and Wallace, 1985) takes the interactions between the fluxes from soil and canopy into account, and is physically sound and rigorous. Previous studies have proved that it performs well for row crops such as maize, wheat, cotton, sorghun and vine (Stannard, 1993; Tourula and Heikinheimo, 1998; Anadranistakis et al., 2000; Teh, et al., 2001; Lund and Soegaard, 2003; Kato et al., 2004; Ortega-Farias et al., 2007; Zhang et al., 2008).

Despite these studies, there are still some insufficiencies in the application of the S-W model (Hu et al., 2009; Zhu et al., 2013). First, the S-W model is sensitive to the errors in the values of canopy and soil resistances (Lund and Soegaard, 2003). Previous studies mainly focused on the parameterization of the canopy resistance (Hanan and Prince, 1997; Samanta et al., 2007; Zhu et al., 2013), and less attentions have been committed to the parameterization of the soil surface resistance (Sellers et

al., 1992; van de Griend and Owe, 1994; Villagarc á et al., 2010). In crop ecosystem, *E* may contribute significantly to the total ET when leaf area index (LAI) is low (Lund and Soegaard, 2003; Zhang et al., 2008). Thus, simultaneous parameterization of the canopy and soil resistances in the S-W model, based on direct measurement of ET and its components by using a combination of micro-meteorological (e.g. eddy covariance methods, Bowen ratio), hydrological (e.g. chambers, microlysimeters) and eco-physiological techniques (e.g. sap-flow, stable isotopes) (Williams et al., 2004; Scott et al., 2006), is important to reduce the model error. However, such studies are relative rare or non-existent. Secondly, as far as the parameterization method is concerned, abundant evidence has shown that the Bayesian method provides a powerful new tool to simultaneously optimize many or all model parameters against all available measurements, and to quantify the influence of uncertainties (Clark and Gelfand, 2006). Although some pioneering efforts have been made (e.g. Samanta et al., 2007; Zhu et al., 2013), the Bayesian method has been much less frequently used in parameterization of ET model than in the other environmental sciences (van Oijen et al., 2005). Moreover, the Bayesian method, to our knowledge, has not been used to simultaneously optimized the parameters of the S-W model against multivariate datasets (section 2.5). Finally, arid northwest China, one of the driest area in the world (Zhu et al., 2007, 2008), is characterized by a widely distributed desert/Gobi interspersed with many oases in different sizes and shapes. Land surface processes of this heterogeneous region are much complex than in other regions (Zhang and Huang, 2004). Thus, the applicability of the S-W model in such regions need to be

92 investigated in details.

93 Based on direct measurements of different components of ET obtained by using
94 the eddy covariance technique and microlysimeters over a spring maize field in the
95 arid region of northwest China from 27 May to 14 September in 2013, the objectives
96 of the present study were to: (1) simultaneously parameterize the S-W model using
97 the Bayesian method against multivariate datasets; (2) verify the performances of the
98 S-W model, and identify the causes of failure and success in simulating ET over the
99 crop ecosystem in arid desert oasis of northwest China. It is expected that this study
100 can not only promote the developments of ET model parameterization, but also help
101 us to find a proper direction in modifying the S-W model used in arid regions.

102 **2 Materials and methods**

103 **2.1 Study site**

104 The study site is located in Daman (DM) Oasis, in the middle Heihe River Basin,
105 Gansu province, China (100^{o} 22’ 20’’ E, 38^{o} 51’ 20’’ N; 1556 m a. s. l; Fig.1). The
106 annual average temperature and precipitation was 7.2 ^{o}C and 125 mm (1960-2000),
107 respectively. The potential evaporation is around 2365 mm year^{-1}, and the dryness
108 index according to the World Atals of Desertification (UNEP, 1992) is 15.9. The soil
109 type is silt clay loam on the surface and silt loam in the deeper layer.

110 The study area has an agricultural development history of over 2000 years owing
111 to its flat terrain, adequate sunlight and convenient water resources from Qilian
112 Mountains. The main crops in the DM Oasis are spring wheat and maize. The spring
113 wheat (*Triticum aestivum* L.) is generally sown in the later March and harvested in the

middle 10 days of July, while the maize (*Zea mays* L.) is sown in the late April and harvested in the middle 10 days of September. Stand density of the spring maize is about 37 plants m^2 with row spacing of 40 cm and planting spacing of 7 cm.

2.2 Measurements and data processing

The field observation systems at this site were constructed in May 2013 as part of the Heihe Watershed Allied Telemetry Experimental Research (HiWATER) project (See details in Li et al., 2013b). The fluxes of sensible heat (H), latent heat (λET) and carbon dioxide were measured at the height 4.5 m using the eddy covariance (EC) system (Liu et al., 2013, manuscript in preparation), which consists of an open-path infrared gas analyzer (Li-7500, LiCor Inc., Lincoln, NE, USA) and a 3D sonic anemometer (CSAT-3, Campbell Scientific Inc., Logan, UT, USA). The EC data were sampled at a frequency of 10 Hz by a data logger (CR5000, Campbell Scientific Inc.), and then were processed with an average time of 30 min. Post-processing calculations, using EdiRe software, included spike detection, lag correction of H_2O/CO_2 relative to the vertical wind component, sonic virtual temperature conversion, planar fit coordinate rotation, the WPL density fluctuation correction and frequency response correction (Xu et al., 2014). About 85% energy balance closure (the sum of $H+\lambda ET$ against the available energy) was found in EC data (Liu et al., 2011). In addition, the flux uncertainties are directly related to the likelihood function of Bayesian inference (Section 2.5). Thus, determining the uncertainties is EC measurements is essential for proper parameter estimates. Recently, Wang et al. (2014) systemically studies the flux uncertainties of EC systems equipped in the HiWATER experiment. Generally,

uncertainties for H ($\sigma_r(H)$; W m^{-2}) by using method of Mann and Lenschow (1994) tended to be $\sigma_r(H) = 0.14H + 2.7$ (R^2=0.95), and uncertainties for λET ($\sigma_r(\lambda ET)$; W m^{-2}) be $\sigma_r(\lambda ET) = 0.13\lambda ET + 6$ (R^2=0.93) (Wang et al., 2014). Data gaps due to instrument malfunction, power failure and bad weather conditions were filled using artificial neural network (ANN) and mean diurnal variations (MDV) methods (Falge et al., 2001). The ANN method was applied when the synchronous meteorological data were available; otherwise, the MDV method was used. The gap-filling data were used only to analyze the seasonal and annual variations in ET.

Continuous complementary measurements also included standard hydro-meteorological variables. Rainfall was measuring using a tipping bucket rain gauge (TE525MM, Campbell Scientific Instruments Inc.). Air temperature, relative humidity (HMP45C, Vaisala Inc., Helsinki, Finland) and wind speed/direction (034B, Met One Instruments, Inc. USA) were measured at heights of 3, 5, 10 15, 20, 30 and 40 m above the ground. Downward and upward solar and longwave radiation (PSP, The EPPLEY Laboratory Inc., USA) and photosynthetic photon flux density (PPFD) (LI-190SA, LI-COR Inc.) were measured at height of 6 m. Soil temperature (Campbell-107, Campbell Scientific Instruments Inc.) and moisture (CS616, Campbell Scientific Instruments Inc.) was measured at 0.02, 0.04, 0.1, 0.2, 0.4, 0.8, 1.2 and 1.6 m depths. Three heat flux plates (HFT3, Campbell Scientific Instruments Inc.) were randomly buried at the depths of 0.01 m. The average soil heat fluxes were calculated using the three randomly buried plates. These data were logged every 10 min by a digital micrologger (CR23X, Campbell Scientific Inc.) equipped with an

158 analog multiplexer (AM416) used for sampling and logging data.

159 Daily soil evaporation was measured using three microlysimeters randomly
160 placed between crop rows (one in the middle of the rows and the other two close to
161 plants on each side of the rows). The microlysimeters with an internal diameter of 10
162 cm and a depth of 20 cm were filled with an intact soil core and pushed into soil with
163 the top slightly above the soil surface (Daamen et al., 1993; Liu et al., 2002). The
164 average weight loss of these microlysimeters measured using electronic scales with
165 0.01 g precision was nearly equal to soil evaporation. In order to keep the soil
166 moisture in microlysimeters similar to that between the rows, the soil in the
167 microlysimeters was replaced daily or every two days.

168 Leaf area index (LAI) was measured using AM300 portable leaf area meter
169 (ADC BioScientific Ltd., UK). The fraction of land cover (f) was estimated by
170 measuring the projected crop canopy area of selected stands in corresponding field
171 plot. LAI, f and crop height were measured approximately every 10 days during
172 the growing season, and the gaps were linearly interpolated to daily interval.

173 **2.3 Description of the S-W model**

174 In the S-W model, the ecosystem evapotranspiration (λET ; W m^{-2}) is separated
175 into evaporation from the soil surface (λE ; W m^{-2}) and transpiration from the
176 vegetation canopy (λT ; W m^{-2}) (Fig. 2), which are calculated as (Shuttleworth and
177 Wallace, 1985; Lhomme et al., 2012):

178 $$\lambda ET=\lambda E+\lambda T = C_s ET_s + C_c ET_c \quad (1)$$

179 $$ET_s = \frac{\Delta A+[\rho C_p D-\Delta r_a^s (A-A_s)]/(r_a^a+r_a^s)}{\Delta+\gamma[1+r_s^s/(r_a^a+r_a^s)]} \quad (2)$$

$$\mathrm{ET_c} = \frac{\Delta A + [\rho C_p D - \Delta r_a^c A_s] / (r_a^a + r_a^c)}{\Delta + \gamma[1 + r_s^c / (r_a^a + r_a^c)]} \quad (3)$$

$$C_s = \frac{1}{1 + [R_s R_a / R_c (R_s + R_a)]} \quad (4)$$

$$C_c = \frac{1}{1 + [R_c R_a / R_s (R_c + R_a)]} \quad (5)$$

$$R_a = (\Delta + \gamma) r_a^a \quad (6)$$

$$R_c = (\Delta + \gamma) r_a^c + \gamma r_s^c \quad (7)$$

$$R_s = (\Delta + \gamma) r_a^s + \gamma r_s^s \quad (8)$$

$$\lambda E = \frac{\Delta A_s + \rho C_p D_0 / r_a^s}{\Delta + \gamma(1 + r_s^s / r_a^s)} \quad (9)$$

$$\lambda T = \frac{\Delta(A - A_s) + \rho C_p D_0 / r_a^c}{\Delta + \gamma(1 + r_s^c / r_a^c)} \quad (10)$$

$$D_0 = D + \frac{(\Delta A - (\Delta + \gamma)\lambda \mathrm{ET}) r_a^a}{\rho C_p} \quad (11)$$

where $\mathrm{ET_s}$ and $\mathrm{ET_c}$ are terms to describe evaporation from soil and transpiration from the plant (W m^{-2}), respectively; C_s and C_c are soil surface resistance and canopy resistance coefficients (dimensionless), respectively; λ is the latent heat of evaporation (J kg^{-1}); Δ is the slope of the saturation vapor pressure versus temperature curve (kPa K^{-1}); ρ is the air density (kg m^{-3}); C_p is the specific heat capacity of dry air (1013 J kg^{-1} K^{-1}); D and D_0 (kPa) are the air water vapor pressure deficit at the reference height (3 m) and the canopy height, respectively; γ is the psychrometric constant (kPa K^{-1}); r_s^c and r_s^s are the surface resistance for plant canopy and soil surface (s m^{-1}), respectively; r_a^c and r_a^s are aerodynamic resistances from the leaf to canopy height and soil surface to canopy height (s m^{-1}), and r_a^a is

aerodynamic resistances from canopy height to reference height (s m^{-1}). A and A_s (W m^{-2}) are the available energy input above the canopy and above the soil surface, respectively, and are calculated as:

$$A = R_n - G \quad (12)$$

$$A_s = R_{ns} - G \quad (13)$$

where R_n and R_{ns} are net radiation fluxes into the canopy and the substrate (W m^{-2}), respectively; G is the soil heat flux (W m^{-2}). R_{ns} was calculated using a Beer's law relationship of the form:

$$R_{ns} = R_n \exp(-K_A \mathrm{LAI}) \quad (14)$$

in which K_A is the extinction coefficient of light attenuation. It can be measured on *site* (see Sauer et al., 2007), and was set to be approximately 0.41 for spring maize (Mo et al., 2000).

The climate-related variables (i.e., λ, e_s, Δ, ρ and γ) in Eqns. (1)-(3) are calculated by the formulas of Allen et al. (1998).

2.4 Calculation of resistances in the S-W model

The resistance network of the S-W model is shown in Fig. 2. In this paper, the three aerodynamic resistance (i.e., r_a^a, r_a^c and r_a^s) were calculated using the same approach suggested by Shuttleworth and Wallace (1985), Shuttleworth and Gurney (1990) and Lhomme et al. (2012).

The canopy resistance (r_s^c), which is the equivalent resistance of all the individual stomates in a canopy and depends on the environmental variables, can be calculated using the Jarvis-type model (Jarvis, 1976)

$$r_s^c = \frac{r_{STmin}}{2LAI\prod_i F_i(X_i)} \quad (15)$$

where r_{STmin} represents the minimal stomatal resistance of individual leaves under optimal conditions. $F_i(X_i)$ is the stress function of a specific environmental variable X_i, with $0 \le F_i(X_i) \le 1$. Following Stewart (1998) and Verhoef and Allen (2000), the stress functions were expressed as:

$$F_1(R_s) = \frac{R_s}{1000}\frac{1000 + k_1}{R_s + k_1} \quad (16)$$

$$F_2(T_a) = \frac{(T_a - T_{a,min})(T_{a,max} - T_a)^{(T_{a,max} - k_2)/(k_2 - T_{a,min})}}{(k_2 - T_{a,min})(T_{a,max} - k_2)^{(T_{a,max} - k_2)/(k_2 - T_{a,min})}} \quad (17)$$

$$F_3(D) = 1 - k_3 D \quad (18)$$

$$F_4(\theta_r) = \begin{cases} 1 & \theta_r > \theta_{cr} \\ \dfrac{(\theta_r - \theta_{wp})}{(\theta_{cr} - \theta_{wp})} & \theta_{wp} \le \theta_r \le \theta_{cr} \\ 0 & \theta_r < \theta_{wp} \end{cases} \quad (19)$$

where $k_1 - k_3$ are constants (units see Table 1); R_s is the incoming solar radiation (W m^{-2}); T_a is the air temperature (^oC) at the reference height; $T_{a,min}$ and $T_{a,max}$ are the lower and upper temperatures limits (^oC), respectively, which are T_a values when $F_2(T_a) = 0$ and are set at values of 0 and 40 ^oC (Harris et al., 2004); θ_r is the actual volumetric soil water content in the root-zone at depth of 0-60 cm (m^3 m^{-3}); θ_{wp} is water content at the wilting point (m^3 m^{-3}); and θ_{cr} is the critical water content (m^3 m^{-3}) at which plant stress starts. The values of θ_{wp} and θ_{cr} are set as 0.11 m^3 m^{-3} and 0.30 m^3 m^{-3} for sandy loam in the study area (Zhao et al., 2010).

The soil surface resistances (r_s^s; Fig. 2) was expressed as a function of near-surface soil water content (Sellers, 1992; Verhoef et al., 2006, 2012; Zhu et al.,

2013):

$$r_s^s = \exp(b_1 - b_2 \frac{\theta_s}{\theta_{sat}}) \quad (20)$$

in which b_1 and b_2 are empirical constants (s m^{-1}); θ_s is soil water content in the top layer of soil (at depth of 2cm); θ_{sat} is the saturated soil water content (m^3 m^{-3}), which was estimated empirically through the near-surface soil texture. In summary, there are 6 site- and species-specific parameters that needed to be estimated in the S-W model associated with soil and canopy resistances, which are b_1, b_2, r_{STmin} and $k_1 - k_3$ (see Appendix A).

2.5 Bayesian inference framework and assimilation scheme

With Bayes' theorem (a complete description was presented in Appendix B), the posterior distribution of parameters $\boldsymbol{c}$ is generated by:

$$p(\boldsymbol{c}|\mathbf{O}) \propto p(\mathbf{O}|\boldsymbol{c})p(\boldsymbol{c}) \quad (21)$$

where $p(\boldsymbol{c})$ represents prior probability distributions of parameters $\boldsymbol{c}$, which is chosen as uniform distributions with specified allowable ranges (Table 1). In general, the parameter ranges were wide enough to include the actual parameter values and to give the optimization freedom (Sack et al., 2006). In the test study, we run the S-W model using 4000 parameter vectors which were sampled from the prior distribution using Latin Hypercube Sampling (LHS) method (Iman and Helton, 1998), and found that the observed data in most case were in the range of predicted values (Appendix A); $p(\mathbf{O}|\boldsymbol{c})$ is the likelihood function, which reflects the influence of the observation datasets on parameter identification; and $p(\boldsymbol{c}|\mathbf{O})$ is the posterior distribution after Bayesian inference conditioned on available observations $\mathbf{O}$.

For each dataset (e.g., λET and *E*), the model-data mismatch $e_i(t)$ $(i=1,2)$, which represents a relative "goodness-of-fit" measure for each possible parameter vector (van Oijen et al., 2011, 2013), is expressed by:

$$e_i(t) = O_i(t) - f_i(t) \tag{22}$$

where $O_i(t)$ and $f_i(t)$ are observed and modeled (equations (1) or (9)) values of the *i*th dataset at time t, respectively. Assuming the model-data mismatch $e_i(t)$ follows a Gaussian distribution with a zero mean, the likelihood function for the *i*th dataset ($\boldsymbol{O}_i(\cdot)$) can be expressed by:

$$p(\boldsymbol{O}_i(\cdot)\,|\,\boldsymbol{c}) = \prod_{t=1}^{n_i} \frac{1}{\sqrt{2\pi}\sigma_i} \mathrm{e}^{-\frac{(e_i(t))^2}{2\sigma_i^2}} \tag{23}$$

where n_i is the number of observations of the *i*th dataset; σ_i $(i=1,2)$ represents the residual errors, or standard deviation about model predicted output of the *i*th dataset. Here, we assumed σ_i is the same over the observation time for the *i*th dataset (Braswell et al., 2005). Traditionally, σ_i can be included into the analysis explicitly (i.e., assuming σ_i is uniform over $\log\sigma_i$; Gelman et al., 1995) and treated as one the model parameters, which yields a complete posterior distribution of σ_i. However, this method artificially increased the parameter dimension of the problem and may result in unreasonable estimations of the parameter values (Kavetski et al., 2006). In this study, σ_i was estimated by using the analytical method (Hurtt and Armstrong, 1996; Braswell et al., 2005), which is to find the value of σ_i that maximizes $\log(p(\boldsymbol{O}_i(\cdot)\,|\,\boldsymbol{c}))$ for a given parameter vector. By differentiating $\log(p(\boldsymbol{O}_i(\cdot)\,|\,\boldsymbol{c}))$ with respect to σ_i, we can obtain:

$$\sigma_i^a = \sqrt{\frac{1}{n_i}\sum_{t=1}^{n_i}(e_i(t))^2} \quad (24)$$

We then used σ_i^a to replace σ_i in the equations (22).

The likelihood function for the multivariate datasets, $p(\boldsymbol{c}\,|\,\mathbf{O})$, used for parameter estimation is then defined as the product of the individual $p(\boldsymbol{O}_i(\cdot)\,|\,\boldsymbol{c})$'s (Richardson et al., 2010):

$$p(\mathbf{O}\,|\,\boldsymbol{c}) = \prod_{i=1}^{m} p(\boldsymbol{O}_i(\cdot)\,|\,\boldsymbol{c}) = \prod_{i=1}^{m}\prod_{t=1}^{n_i} \frac{1}{\sqrt{2\pi}\sigma_i} e^{-\frac{(e_i(t))^2}{2\sigma_i^2}} \quad (25)$$

where m is the number of dataset; When a particular dataset $\boldsymbol{O}_i(\cdot)$ was not being used in the optimization, we simply set the corresponding likelihood function $p(\boldsymbol{O}_i(\cdot)\,|\,\boldsymbol{c})$ to 1. Thus, this framework can be easily used when additional observations are available. In this studies, the two datasets used to simultaneously optimize the parameter values were: EC-measured half-hourly evapotranspiration (λET; Wm^{-2}) and microlysimeters-measured daily soil evaporation (E; mm d^{-1}).

2.6 Metropolis-Hasting algorithm and convergence test

The posterior distribution was sampled using the Metropolis–Hasting (M-H) algorithm (Metropolis et al., 1953; Hastings, 1970), a version of the Markov Chain Monte Carlo (MCMC) technique. To generate a Markov chain in the parameter space, the M-H algorithm was run by repeating two steps: a proposing step and a moving step. In the proposing step, a candidate point $\boldsymbol{c}^{\text{new}}$ is generated according to a proposal distribution $P(\boldsymbol{c}^{\text{new}}\,|\,\boldsymbol{c}^{k-1})$, where $\boldsymbol{c}^{k-1}$ is the accepted point at the previous step. In the moving step, point $\boldsymbol{c}^{\text{new}}$ is treated against the Metropolis criterion to examine if it should be accepted or rejected. It was well recognized that efficiency of

the M-H algorithm was strongly effected by the proposal distribution function. To find an effective proposal distribution $P(\boldsymbol{c}^{\text{new}} \mid \boldsymbol{c}^{k-1})$, a test run of the M-H algorithm with 10, 000 simulations was made by using a uniform proposal distribution (Braswell et al., 2005):

$$\boldsymbol{c}^{\text{new}} = \boldsymbol{c}^{k-1} + r(\boldsymbol{c}^{\max} - \boldsymbol{c}^{\min}) \tag{26}$$

where $\boldsymbol{c}^{k-1}$ is the current accepted point; r is a random number uniformly distributed between -0.5 and +0.5; $\boldsymbol{c}^{\min}$ and $\boldsymbol{c}^{\max}$ are the lower and upper limits of parameter vector $\boldsymbol{c}$ (Table 1). Based on the test run, we then constructed a normal proposal distribution $\boldsymbol{c}^{\text{new}} \sim N(\boldsymbol{c}^{(k-1)}, \text{cov}^0(\boldsymbol{c}))$, where $\text{cov}^0(\boldsymbol{c})$ is the covariance matrix of the parameter vector $\boldsymbol{c}$ from the initial test run (Xu et al., 2006). The detailed description on MCMC sampling procedure and the code written in Matlab were presented in Appendix B.

We ran at least four parallel MCMC chains with 20,000 iterations each, evaluated the chain convergence using the Gelman-Rubin (G-R) diagnostic method (Gelman and Rubin, 1992) (Appendix C), and thinned the chains (every 20th iteration) when appropriate to reduce within chain autocorrelation, thereby producing an independent sample of 3000 values for each parameter from the joint posterior distribution.

2.6 Evaluation of model output estimates

Since the primary interest in application of the S-W model was to reproduce the pattern of water vapour fluxes from different sources (i.e., soil and vegetation) during the whole study period, we used all available data to construct the likelihood function

(equation 25) and to obtain the posterior distribution of the parameters. Then, the performance of the S-W model was evaluated using the coefficient of determination of the linear regression between measured and estimated values of water vapor fluxes, R^2, representing how much the variation in the observations was explained by the models. Also, the root mean square error (RMSE), mean bias error (MBE), index of agreement (IA) and model efficiency (EF) (Legates and McCabe, 1999; Poblete-Echeverria & Ortega-Farias, 2009) were included in the statistical analysis, which are calculated as follows:

$$\mathrm{RMSE}=\sqrt{\frac{1}{n_i}\sum_{t=1}^{n_i}[O_i(t)-f_i(t)]^2} \tag{26}$$

$$\mathrm{MBE}=\frac{1}{n_i}\sum_{t=1}^{n_i}[O_i(t)-f_i(t)] \tag{27}$$

$$\mathrm{IA}=1-\frac{\sum_{t=1}^{n_i}[O_i(t)-f_i(t)]^2}{\sum_{t=1}^{n_i}[|O_i(t)-\overline{O_i}|+|f_i(t)-\overline{O_i}|]^2} \tag{28}$$

$$\mathrm{EF}=1-\frac{\sum_{t=1}^{n_i}[O_i(t)-f_i(t)]^2}{\sum_{t=1}^{n_i}[O_i(t)-\overline{O_i}]^2} \tag{29}$$

where n_i is the total number of observations of the *i*th dataset; $O_i(t)$ is the observed values at time t of the *i*th dataset, $\overline{O_i}$ is the mean of the observed value of the *i*th dataset, and $f_i(t)$ is the simulation which was calculated using the posterior median parameter values, and other parameter vectors selected from the parameter chains generated by the MCMC iteration (van Oijen et al., 2013).

3 Results

3.1 Environmental and biological factors

Detailed information on the seasonality of key environmental and biological variables is essential to assess seasonal variation in the actual ET and its partitioning. The seasonal change in net solar radiation (R_n; MJ m^{-2} d^{-1}), air temperature (T_a; ^oC), air water vapor pressure deficit (D; kPa), wind speed (u, m s^{-1}) at the height of 3 m, rainfall and irrigation (mm), soil water content (θ; m^3 m^{-3}), and leaf area index (LAI; m^2 m^{-2}) are illustrated in Fig. 3. During the study period (DOY147-257), the daily mean R_n varied from 2.6 to 18.5 MJ m^{-2} d^{-1} with an average value of 11.9 MJ m^{-2} d^{-1}. The peaked values were recorded from the end of June to the middle of July (DOY180-195). The variation of mean daily air temperature (T_a) has a similar trend to R_n, varying from 8.8 to 24.9 ^oC with an average value of around 19.0 ^oC. D exhibited large diurnal variation ranging from 0 to 3.5 kPa, and the daily mean D was relative small when the LAI was larger than 3 m^2 m^{-2} (DOY197-230). Daily mean wind speed (u) ranged from 0.5 to 3.2 m s^{-1}, and was close to normal long-term values. Total precipitation during the study period was 104.2 mm with eight events over 5.0 mm (Fig. 3). θ varied greatly over the whole growing season. The variability of θ mainly depended on irrigation scheduling of local government (irrigation quota and timing). Soil water content had a peak value (about 0.35 m^3 m^{-3}) after irrigation and gradually reduced till the next irrigation (Fig. 3). The LAI showed a clear ‘one peak’ pattern over the whole growing season with relative high values of 3.5 m^{-2} m^{-2} from early July to late August (DOY184-221).

3.2 Posterior distribution of S-W model parameters

366 The posterior parameter distributions are shown as histograms in Fig. 4 and
367 summarized in Table 1 by posterior medians and 95% probability intervals. The
368 results showed that the Bayesian calibration against the multivariate datasets was in
369 most cases successful in reducing the assumed prior ranges of the parameters values.
370 Parameters r_{STmin}, b_1, b_2 and k_2 showed relatively large uncertainty reductions
371 (defined as $1-\mathrm{CI}_{posterior}/\mathrm{CI}_{prior}$, where CI is the length of the 95% credible interval)
372 (Fig. 5), and their posterior distributions became approximately symmetric with
373 distinctive modes, while parameters k_1 and k_3 have relative large variability
374 (widely spread on the prior bounds) (Fig. 4). The global sensitivity analysis with the
375 first-order impact ratio (FOIR) values (Appendix A) reveals the importance of input
376 parameters in affecting total ecosystem evapotranspiration. The results indicated that
377 total ET responded sensitively to r_{STmin}, b_1, b_2 and k_2 with FOIR values being
378 54.3%, 21.9%, 10.4% and 8.5% (Appendix A), respectively. Other parameters
379 exhibits relative low (<5%) FOIR values, suggesting that the variability in these
380 parameters had almost no effect on the variability in model output. It is worth noting
381 that the four highest sensitive parameters (r_{STmin}, b_1, b_2 and k_2) also corresponded
382 to the greatest degree of updating in the Bayesian inference. Thus, we thought that the
383 key parameters in the S-W model were well optimized by the Bayesian method
384 against the multivariate datasets. In addition, the correlation coefficient between the
385 posterior distribution of parameters can be used to find groups of parameters tend to
386 be constrained together (Knorr and Kattge, 2005). In this study, the six calibrated
387 parameters were not significantly inter-correlated with each other with correlation

388 coefficients lower than 0.1 (Appendix B).

389 The responses of soil surface resistances (r_s^s) to soil water content computed
390 using our posterior mean b_1 and b_2 values were very similar to that calculated using
391 equation developed by Ortega-Farias et al. (2010) based on direct soil evaporation
392 measurements, but seemed to be more sensitive to changes in soil water content
393 compared with some other studies (e.g., Sun, 1982; Sellers, 1992; Zhu et al., 2013;
394 Fig. 6). When just using EC-measured λET data, a relative wider posterior distribution
395 of b_2 was observed (see Appendix B). Thus, the daily soil evaporation data helped to
396 well constrain estimates of b_1 and b_2. The posterior mean value of r_{STmin} from our
397 study was very close to that (20 s m^{-1}) reported for spring maize growing in
398 northwest China obtained by using the least squares fitting method(Li et al., 2013a).
399 The variations of the minimal stomatal resistance (r_{STmin}) for many natural and
400 cultivated plants have been widely investigated by previous studies (Korner et al.,
401 1979; Pospisilova and Solarova, 1980). Typical values for r_{STmin} vary considerably
402 from about 20-100 s m^{-1} for crops to 200-300 s m^{-1} for many types of trees. Thus, our
403 results fell within the range of previous studies. However, some parameters related to
404 canopy surface resistance (i.e., k_1 and k_3) seemed to be not well updated (Fig. 4). This
405 may be due to the fact that these parameters may be insensitive to the present
406 available datasets.

407 **3.3 Model performance compared with measurements**

408 Having parameterized the S-W model as described above, we ran the model to
409 simulate the half-hourly λET (equation 1) and λE (equation 9) values (W m^{-2}). The

daily estimations of evapotranspiration (ET; mm d^{-1}) and soil evaporation (E ; mm d^{-1}) were obtained by summing up the half-hourly simulated values. The statistical analysis of observed versus estimated values of water vapor fluxes at different time-scales are summarized in Table 2. These results indicated that the parameterized S-W model was able to predict λET on a half-hourly basis with values of R^2, IA and EF equal to 0.83, 0.93 and 0.74, respectively. However, significant differences exist between measured and modeled half-hourly λET values for the spring maize in the arid desert oasis. The slope (0.84) of regression equation between the measured and modeled half-hourly λET values was lower than one (Table 2 and Fig. 7a), which indicated that the S-W model tended to underestimate the half-hourly λET with a MBE value of 24.2 W m^{-2}. Ortega-Farias et al. (2010) also reported that the S-W model underestimated on half-hourly time intervals compared the EC-measured λET over a drip-irrigated vineyard in Mediterranean semiarid region during the growing season in 2006. On the contrary, some studies showed that the S-W model overestimated half-hourly λET (e.g., Li et al., 2013a; Ortega-Farias et al., 2007; Zhang et al., 2008). Therefore, the performances of the S-W model seemed to be variable for different crops and places, and there is a need to identify the causes that induced the disagreements between observed and modeled values (discussed below).

The fluctuation of measured and estimated daily ET and E is illustrated in Fig. 8. In this case, a good agreement between measured and estimated daily E was obtained with values of R^2, IA and EF equal to 0.82, 0.94 and 0.76 (Table 2). The points in plots of measured-versus-modeled daily E fell tightly along the 1:1 line (slope=1.01

and intercept=0.01 with RMSE=0.05 and MBE=-0.01; Fig. 7b and Table 2). Also, the 95% posterior prediction intervals of simulated soil *E* was narrow. Thus, we thought that the soil resistance in the S-W model was properly parameterized for the spring maize by the measured soil evaporation data. From Fig. 8, we can also observe that the estimated daily ET generally fluctuated tightly with the measured values with relative narrow uncertainties (95% posterior predication intervals). The values of RMSE, MBE, IA and EF were equal to 0.05, 0.14 mm d^{-1}, 0.94 and 0.79, respectively (Table 2). However, there are 12 days during the study period (111 days) with observations beyond the upper bounder of the 95% posterior predication intervals (Fig. 8). For example, on the 5^{th} of July, the estimated using the median values of the parameters and measured daily ETs were 2.9 and 4.3 mm d^{-1}, respectively (Fig. 8). Thus, the causes of the underestimations of ET by the S-W on these days needs to be carefully checked based on detailed micrometeorological data. This work would help us to modify the model in a correct way and improve the precision of prediction.

3.4 Identification of the disagreement/agreement between observed and modeled ET values

The diurnal variation of R_n, H and λET (measured and modeled) above the spring maize ecosystem for some selected days is presented in Fig. 9. The uncertainties of H and λET increased with the flux magnitude (Fig. 9), and tended to be approximately 14% and 13%, respectively (Wang et al., 2014). The relative error for R_n was relatively small and estimated to be 1.24% (Xu et al., 2013). Resulting from the high surface heterogeneities, one special phenomenon, known as the “oasis

454 effect" (Lemon et al., 1957; Oke, 1978) or "cold island effect" (Wang et al., 1992;
455 Zhang and Huang, 2004), was often observed on clear days in July and August in the
456 study area and it is characterized as follows: (1) H is very small and even negative
457 (downward) in the afternoon (Figs. 9a-c) due to the micro-scale advection of hot dry
458 air over the desert to crop surface in the oasis (Oke, 1978; Hu et al., 1994). For an
459 example, on the 5th of July, H was continuously negative from 12 : 00 to 20 : 00 (Fig.
460 9a). A strong advection process can be distinctly detected from the temperature and
461 relative humidity profiles (Figs. 10a and 10b), in which the highest temperature
462 occurred at a height of 8-18 m; (2) measured actual λET often exceeded (Fig. 9a) or
463 was equal to (Figs. 9b and 9c) the local net radiation because of the added energy in
464 the form of downward fluxes of H to the ET process (Evett et al., 2012). Under such
465 conditions, the S-W model significantly underestimated the actual ET values due to
466 the real atmospheric flows that do not correspond to its assumption of horizontal
467 homogeneities (Rao et al., 1974). Thus, how to properly represent the advection
468 process in the S-W model should be paid special attention in simulating ET over crop
469 ecosystems in arid desert oasis in the future studies. In addition to this situation, slight
470 underestimations were also observed on or shortly after rainy days (Fig. 8). For
471 example, the simulated half-hourly λET was lower than that measured by EC after the
472 rainfall event occurred in 13 : 00 on 17 June (Fig. 9d). We thought that the
473 underestimations by the model on or shortly after rainy days were mainly due to
474 ignoring the direct evaporation of liquid water intercepted in the crop canopy, because
475 no downward H and temperature inversion were observed on this day (Figs. 10c and

476 10d). Until now, several canopy interception models have been developed (e.g., Rutter
477 et al., 1971; Mulder, 1985; Gash et al., 1995; Bouten et al., 1996). However, many of
478 them were developed for simulating the rainfall interception by forest ecosystems, and
479 their suitability for crops need to be further investigated.

480 The diurnal variation of simulated half-hourly λET by the parameterized S-W
481 model has a similar trend to the measurements on clear and advection-absent days
482 during the whole study periods (Figs. 9e-h). On these days, *H* was positive (upwards)
483 at day time (Figs. 9e-h) and no temperature inversion was observed (Figs. 10e and
484 10f). Thus, we thought that the parameterization schedule adopted in this study
485 worked well. It also demonstrated that the properly parameterized S-W model can be
486 used in simulating and partitioning ET for homogeneous land surface. Hu et al. (2009)
487 reported that the S-W model parameterized by using Monte Carlo method can
488 successfully simulated ET at four uniform grasslands in China; Our previous studies
489 (Zhu et al., 2013) also illustrated that parameterized S-W model can be used to
490 simulate and partition ET over a vast alpine grassland in Qinghai-Tibet Plateau.

491 **4 Discussion**

492 The assessment of model errors remains an outstanding challenge in Hydrology
493 (Beven, 2008). Identifying the uncertainties related to model parameter and structure
494 needs to take on a prominent position in the hydrological modeling (Bastola et al.,
495 2011; Brigode et al., 2013). An important issue in identifying the parameter
496 uncertainty is equifinality, where different parameters of the same model yield similar
497 results, and so can be difficult to distinguish which is correct (see Franks et al., 1997).

A variety of recent studies corroborated the multi-objective calibration against the multiple (orthogonal; see Winsemius et al., 2006) datasets can produce a robust parameter estimates (e.g., Engeland et al., 2006; Fenicia et al., 2007; Moussa and Chahinian, 2009; Richardson et al., 2010; Hrachowitz et al., 2013). In this study, we constructed a Bayesian inference framework to constrain the model parameters using the EC-measured ET and microlysimeters-measured daily *E* datasets simultaneously. The results indicated that 4 of the six main parameters were considerably updated, and simulated λET and *E* were comparable to the measurements with relatively narrow uncertainties (95% posterior predication intervals). Using just EC-measured ET data in our test study (see Appendix B), the optimized S-W model on the simulations of λET were not significantly different from that optimized by multivariate datasets procedure, but it significantly underestimated *E* with great uncertainties (Appendix B). Thus, we can not ensure the S-W model optimized using only the EC-measured ET data can properly partition the total ET into its different components (soil evaporation and plant transpiration), even thought the simulated λET values were in good agreement with measurements. Limited success in estimating process-based model parameters using EC-measured data alone were also reported in previous studies (e.g., Wang et al., 2001; Knorr and Kattge, 2005; Richardson et al., 2010).

With the developments of observation technologies and strategies, major steps forwards have been made in extracting a wide variety of environmental data (Hrachowitz et a., 2013). Thus, it is critical to assess to what extent the uncertainty in model parameters and model predictions is reduced by the use of additional data and

what new observation is required. The Bayesian inference framework used in this study provided a convenient way to simultaneously constrain model parameters when the new observation datasets are available. However, even with all datasets (EC-measured λET and microlysimeters-measured daily E), some parameters related to canopy surface resistance seemed to be not well updated (Fig. 4). We thought that this may be due to the insensitivities of these parameters (e.g., k_1, k_3, T_{amax}, T_{amin} and K_A) to the present available datasets. Thus, direct observations of plant transpiration using sap flow or stable isotope (δ^2H and $\delta^{18}O$) technologies (see Williams et al., 2004), canopy temperature using infrared thermometer and continuous within- and above-canopy radiation using the four-component net radiometer (see Sauer et al., 2007) are needed in the future studies.

The method, as implemented here, used all observations simultaneously to constrain parameters and obtain an optimal match between data and model. After parameter optimizing, the main source of model error can be attributed to the model structure. Thus, this method facilitates the detection of the model structural failures. Until now, numerous models, retaining the S-W model as basis, have been developed for estimating ET or its different components, and they tended to be more and more complex (see Lhomme et al., 2012). However, increasing model complexity is always accompanied by a great danger of equifinality and large uncertainties in forward runs (Beven et al., 1989; Franks and Beven, 1997). Most importantly, we must ensure that we are on the right direction in modifying the model. In this study, we found that the S-W model applied in arid areas generally failed when local advection occurred (Fig.

9). Thus, we thought that the main structural error of the S-W model as well as its various extensions comes from the ignorance of the effects of advection on the ET processes. A potential solution is to add the additional energy (negative *H*) to the available energy term defined in equation 12 (see Parlange and Katul, 1992).

The distribution of the model-minus-observation residuals, through the likelihood function, may also have an influence on the estimation of posterior parameter distributions (Raupach et al., 2005). However, a *priori* assessment of these errors may be not easy (Beven, 2001). Fig. 11 shows the distribution of the residuals between simulated and observed datasets. The results indicated that the model-minus-observation departures of half-hourly λET flux was better approximated by a double-exponential distribution, which was in agreement with previous studies (Hollinger and Richardson, 2005; Richardson et al., 2006). Thus, the two-tower approach (Hollinger and Richardson, 2005), which can give a prior estimates of the flux data uncertainties, should be applied in the Bayesian inference in future studies. The Cauchy distribution gave a more appropriate approximation for the daily *E* departures. However, the Cauchy distribution may be not a good choice for the purpose of Bayesian inference, since its first four moments are undefined (Richardson et al., 2008).

5 Conclusions

This study illustrated the use of the Bayesian method to simultaneously parameterize a two-source ET model against the multivariate datasets for a crop ecosystem in a desert oasis of northwest China. The posterior distributions of the

model parameters in most cases can be well constrained by the observations. Generally, the parameterized model has a good performance in simulating and partitioning ET. However, underestimations were observed on days when the 'oasis-effect' occurred. Therefore, in the future studies, special attentions should be given to proper descriptions of the effects of advection on estimating ET for heterogeneous land surface. In addition, the canopy interception model should be coupled with the two-source ET model in long-term simulation.

Acknowledgements

The eddy covariance flux, meteorological, and other data used in this study are from Heihe Watershed Allied Telemetry Experimental Research (HiWATER) (http://heihedata.org/hiwater). We thank all the scientists, engineers and students who participated in HiWATER field campaigns. This research was supported by National Natural Science Foundation of China (No. 31370467), the Chinese Academy of Sciences Action Plan for West Development Program Project (KZCX2-XB3-15) and New Century Excellent Talents in University of Chinese Ministry of Education (No. NCET-11-0219).

References

Allen, R.G., Pereira, L.S., Raes, D., Smith, M.: Crop evapotranspiration- guidelines for computing crop water requirements. FAO Irrigation and Drainage Paper, No. 56, FAO, Rome, 1998.

Anadranistakis, M., Liakatas, A., Kerkides, P., Rizos, S., Gavanosis, J., Poulovassilis, A.: Crop water requirements model tested for crops grown in Greece. Agr. Water

586 Manage., 45 (3), 297-316, 2000.
587 Bastola, S., Murphy, C., Sweeney, J.: The role of hydrological modelling uncertainties
588 in climate change impact assessments of Irish river catchments. Adv. Water
589 Resour., 34, 562-576, 2011.
590 Beven, K.: Changing ideas in hydrology-The case of physically-based model. J.
591 Hydrol., 105, 157-172, 1989.
592 Beven, K.: How far can we go in distributed hydrological modelling ? Hydrol. Earth
593 Syst. Sci., 5(1), 1-12, 2001.
594 Beven, K.J., Smith, P.J., Freer, J.E.: So just why would a modeller choose to be
595 incoherent? J. Hydrol., 354, 15-32, 2008.
596 Bouten, W., Schaap, M.G., Aerts, J., Vermetten, A.W.M.: Monitoring and modelling
597 canopy water storage amounts in support of atmospheric depositions studies. J.
598 Hydrol., 181: 305-321, 1996.
599 Braswell, B., Sacks, W.J., Linder, E., Schimel, D.S.: Estimating diurnal to annual
600 ecosystem parameters by synthesis of a carbon flux model with eddy covariance
601 net ecosystem exchange observations. Global Change Biol., 11, 1-21, 2005.
602 Brigode a, P., Oudin, L., Perrin, C.: Hydrological model parameter instability: A
603 source of additional uncertainty in estimating the hydrological impacts of climate
604 change? J. Hydrol., 476, 410-425, 2013.
605 Clark, J.S., Gelfand, A.E.: A future for models and data in environmental science.
606 Trends Ecol. Evol., 12, 375-380, 2006.
607 Daamen, C., Simmonds, L.E., Wallace, J.S., Laryea, K.B., Sivakumar, M.U.K.: Use

608 microlysimeters to measure evaporation from sandy soils. Agric. For. Meteor., 65,
609 159-173, 1993.
610 Engeland, K., Braud, I., Gottschalk, L., Leblois, E.: Multi-objective regional
611 modeling. J. Hydrol., 327, 339-35, 2006.
612 Evett, S.R., Kustas, W.P., Gowda, P.H., Anderson, M.A., Prueger, J.H., Howell, T.A.:
613 Overview of the Bushland Evapotranspiration and Agricultural Remote sensing
614 EXperiment 2008 (BEAREX08): A field experiment evaluating methods for
615 quantifying ET at multiple scales. Adv. Water Resour., 50, 4-19, 2012.
616 Fenicia, F., Savenije, H.H.G., Matgen, P., Pfister, L.: A comparison of alternative
617 multiobjective calibration strategies for hydrological modeling. Water Resour.
618 Res., 43, W03434, 2007.
619 Ferretti, D., Pendall, E., Morgan, J., Nelson, J., LeCain, D., Mosier, A.: Partitioning
620 evapotranspiration fluxes from a Colorado grassland using stable iostopes:
621 seasonal variations and ecosystem implications of elevated atmospheric CO_2.
622 Plant and Soil, 254(2), 291-303, 2003.
623 Flumignan, D.L., Faria, R.T., Prete, C.E.C.: Evapotranspiration components and dual
624 crop coefficients of coffee trees during crop production. Agr. Water Manage., 98,
625 791-800, 2011.
626 Franks, S.W., Beven, K.J., Quinn, P.F., Wright, I.R.: On the sensitivity of
627 soil-vegetation-atmosphere transfer (SVAT) schemes: equifinality and the
628 problem of robust calibration. Agric. For. Meteorol., 86, 63-75, 1997.
629 Franks, S.W., Beven, K.J.: Bayesian estimation of uncertainty in land

surface-atmosphere flux predictions. J. Geophys. Res. Atmos., 102, 23991-23999, 1997.

Gash, J.H.C., Lloyd, C. R., Lachaud, G., Estimating sparse forest rainfall interception with an analytical model. J. Hydrol., 170, 79-86, 1995.

Gelman, A., Rubin, D.B. Inference from Iterative Simulation Using Multiple Sequences. Statistical Sciences, 7, 457-511, 1992.

Gelman, A.B., Carlin, J.S., Stern, H.S. Rubin, D.B.: Bayesian Data Analysis. Texts in Stat. Sci. Ser., edited by C. Chatfield and J.V. Zidek, CRC Press, Boca Raton, Florida, 1995.

Hanan, N.P., Prince, S.D.: Stomatal conductance of west-central supersite vegetation in HAPEX-Sahel: measurements and empirical model. J. Hydrol., 188-189, 536-562, 1997.

Harris, P.P., Huntingford, C., Cox, P.M., Gash, J.H.C., Malhi, Y.: Effect of soil moisture on canopy conductance of Amazonian rainforest. Agric. For. Meteor., 122, 215-227, 2004.

Hastings, W.K.: Monte Carlo sampling methods using Markov chains and their applications. Biometrika, 57, 97-109, 1970.

Hollinger, D.Y., Richardson, A.D.: Uncertainty in eddy covariance measurements and its application to physiological models. Tree Physiol., 25, 873-885, 2005.

Hrachowitz, M., Savenije, H., Bogaard, T.A., Tetzlaff, D., Soulsby, C.: What can flux tracking teach us about water age distribution patterns and their temporal dynamics? Hydrol. Earth Syst. Sci., 17, 533-564, 2013.

652 Hrachowitz, M., Savenije, H.H.G., Blöschl, G., McDonnell, J.J., Sivapalanf, M.,
653 Pomeroy, J.W., Arheimer, B., Blumei, T., Clark, M.P., Ehret, U., Feniciaal, F.,
654 Freer, J.E., Gelfann, A., Guptao, H.V., Hughes, D.A., Hut, R.W., Montanari, A.,
655 Pandea, S., Tetzlaff, D., Trocho, P.A., Uhlenbrook, S., Wagener, T., Winsemius,
656 H.C., Woods, R.A., Zehek, E., Cudennec, C.: A decade of Predictions in
657 Ungauged Basins (PUB)- a review. Hydrolog. Sci. J., 58(6), 1198-1255, 2013.
658 Hu, Y.Q.: Research advance about the energy budget and transportation of water
659 vapour in the HEIFE area. Advance in Earth Science, 9(4), 30-34, 1994. (in
660 Chinese with English abstract).
661 Hu, Z.M., Yu, G.R., Zhou, Y.L., Sun, X.M., Li, Y.N., Shi, P.L., Wang, Y.F., Song, X.,
662 Zheng, Z.M., Zhang, L., Li, S.G.: Partitioning of evapotranspiration and its
663 controls in four grassland ecosystems: Application of a two-source model. Agric.
664 For. Meteor., 149, 1410-1420, 2009.
665 Iman, R.L., Helton, J.C.: An investigation of uncertainty and sensitivity analysis
666 techniques for computer models. Risk Anal., 8(1), 71-90, 1988.
667 Jarvis, P.G.: The interpretation of the variations in leaf water potential and stomatal
668 conductance found in canopies in the field. Philos. T. R. Soc. B., 273, 563-610,
669 1976.
670 Kato, T., Kimura, R., Kamichika, M.: Estimation of evapotranspiration, transpiration
671 ratio and water-use efficiency from a sparse canopy using a compartment model.
672 Agr. Water Manage., 65 (3), 173-191, 2004.
673 Kavetski, D., Kuczera, G., Franks, S.W.: Bayesian analysis of input uncertainty in

674 hydrological modeling: 1. Theory. Water Resour. Res., 42, W03407,
675 doi:10.1029/2005WR004368, 2006.
676 Knorr, W., Kattge, J.: Inversion of terrestrial ecosystem model parameter values
677 against eddy covariance measurements by Monte Carlo sampling. Global Change
678 Biol., 11, 1333-1351, 2005.
679 Korner, C., Schecl, J.A., Bauer, H. Maximum leaf diffusive conductance in vascular
680 plants. Phorosynrherica, 13, 45-82, 1979.
681 Legates, D.R., McCabe, G.J.: Evaluating the use of 'goodness-of-fit' measures in
682 hydrologic and hydroclimatic model validation. Water Resour. Res., 35, 233-241,
683 1999.
684 Lemon, E.R., Glaser, A.H., Satterwhite, L.E.: Some aspects of the relationship of soil,
685 plant, and meteorological factors to evapotranspiration. Proc. Soil Sci. Soc. Amer.,
686 21, 464-468, 1957.
687 Lhomme, J.P., Montes, C., Jacob, F., Prévot, L.: Evaporation from Heterogeneous and
688 Sparse Canopies: On the Formulations Related to Multi-Source Representations.
689 Boundary-Layer Meteorol., 144, 243–262, 2012.
690 Lhomme, J.P., Montes, C., Jacob, F., Prévot, L.: Evaporation from Heterogeneous and
691 Sparse Canopies: On the Formulations Related to Multi-Source Representations.
692 Boundary-Layer Meteorol., 144, 243-262, 2012.
693 Li, S.E., Kang, S.Z., Zhang, L., Ortega-Farias, S., Li, F.S., Du, T.S., Tong, L., Wang,
694 S.F., Ingman, M., Guo, W.H.: Measuring and modeling maize evapotranspiration
695 under plastic film-mulching condition. J. Hydrol., 503, 153-168, 2013a.

Li, X., Cheng, G.D., Liu, S.M., Xiao, Q., Ma, M.G., Jin, R., Che, T., Liu, Q.H., Wang, W.Z., Qi, Y., Wen, J.G., Li, H.Y., Zhu, G.F., Guo, J.W., Ran, Y.H., Wang, S.G., Zhu, Z.L., Zhou, J., Hu, X.L., Xu, Z.W.: Heihe Watershed Allied Telemetry Experimental Research (HiWATER): Scientific objectives and experimental design1. B. Am. Meteorol. Soc., 94(8), 1145-1160, 2013b.

Liu, C.M., Zhang, X.Y., Zhang, Y.Q.: Determination of daily evaporation and evapotranspiration of winter wheat and maize by large-scale weighing lysimeter and micro-lysimeter. Agric. For. Meteor., 111, 109-120, 2002.

Liu, S.M., Xu, Z.W., Wang, W.Z., Jia, Z.Z., Zhu, M.J., Bai, J., Wang, J.M.: A comparison of eddy-covariance and large aperture scintillometer measurements with respect to the energy balance closure problem. Hydrol. Earth Syst. Sci., 15, 1291-1306, 2011.

Lund, M.R., Soegaard, H.: Modelling of evaporation in a sparse millet crop using a two-source model including sensible heat advection within the canopy. J. Hydrol., 280, 124-144, 2003.

Mann, J., Lenschow, D.H.: Errors in airborne flux measurements. J. Geophys. Res., 99, 14519-14526, 1994.

Metropolis, N.R., Rosenbluth, A.W., Rosenbluth, M.N., Teller, A.H.: Equations of state calculations by fast computing machines. J. Chem. Phys., 21, 1087-1091, 1953.

Mo, X.G., Lin, Z.H., Xiang, Y.Q., Liu, S.X.: Characteristics of incoming radiation through maize canopy. Eco-agriculture Research, 8, 1-4, 2000.

718 Morison, J.I.L., Baker, N.R., Mullineaux, P.M., Davies, W.J.: Improving water use in
719 crop production. Phil. Trans. R. Soc. B., 363, 639-658, 2008.
720 Moussa, R., Chahinian, N.: Comparison of different multi-objective calibration
721 criteria using a conceptual rainfall–runoff model of flood events. Hydrol. Earth
722 Syst. Sci., 13, 519-535, 2009.
723 Mulder, J.P.M.: Simulating interception loss using standard meteorological data. The
724 Forest-Atmosphere Interaction, B. Hutchison and B. Hicks, Eds., D. Reidel,
725 177-196, 1985.
726 Noilhan, J., Planton, S.: A simple parameterization of land surface processes for
727 meteorological Models, Mon. Weather Rev., 117, 536-549, 1989.
728 Ogink-Hendriks, M.J.: Modelling surface conductance and transpiration of an
729 oak forest in the Netherlands. Agric. For. Meteorol., 74, 99-118, 1995.
730 Oke, T. R.: Boundary layer Climates. Second edn. Mathuen, London, 1978.
731 Ortega-Farias, S., Carrasco, M., Olioso, A., Acevedo, C., Poblete, C.: Latent heat flux
732 over a Cabernet Sauvignon vineyard using the Shuttleworth and Wallace model.
733 Irrig. Sci., 25, 161-170, 2007.
734 Ortega-Farias, S., Poblete-Echeverria, C., Brisson, N.: Parameterization of a two-layer
735 model for estimating vineyard evapotranspiration using meteorological
736 measurements. Agric. For. Meteor., 150, 276-286, 2010.
737 Parlange, M.B., Katul, G.G.: An advection-aridity evaporation model. Water Resour.
738 Res., 28(1), 127-132, 1992.
739 Poblete-Echeverria, C., Ortega-Farias, S.: Estimation of actual evapotranspiration for

740 a drip-irrigated Merlot vineyard using a three-source model. Irrigation Sci., 28,
741 65-78, 2009.
742 Pospisilova, J., Solarova, J.: Environmental and biological control of diffusive
743 conductance of adaxial and abaxial leaf epidermis. Photosyntherica, 14, 90-127,
744 1980.
745 Rana, G., Katerji, N.: Measurement and estimation of actual evapotranspiration in
746 the field under Mediterranean climate: a review. Eur. J. Agron., 13(2-3), 125-153,
747 2000.
748 Rao, K., Wyngaard, J., Cote, O.: Local advection of momentum, heat, and moisture in
749 micrometeorology. Boundary-Layer Meteorol., 7(3), 331-348, 1974.
750 Raupach, M.R., Rayner, P.J., Barrett, D.J., Defries, R.S., Heimann, M., Ojima, D.S.,
751 Quegan, S., Schmullius, C.C.: Model-data synthesis in terrestrial carbon
752 observation: methods, data requirements and data uncertainty specifications.
753 Global Change Biol., 11, 378-397, 2005.
754 Richardson, A.D., Hollinger, D.Y., Burba, G.G., Davis, K.J., Flanagan, L.B., Katul,
755 G.G., Williammunger, J., Ricciuto, D.M., Stoy, P.C., Suyker, A.E., Verma, S.B.,
756 Wofsy, S.C.: A multi-site analysis of random error in tower-based measurements
757 of carbon and energy fluxes. Agric. For. Meteor., 136, 1-18, 2006.
758 Richardson, A.D., Mahecha, M.D., Falge, E., Kattge, J., Moffat, A.M., Papale, D.,
759 Reichstein, M., Stauch, V.J., Braswell, B.H., Churkina, G., Kruijt, B., Hollinger,
760 D.Y.: Statistical properties of random CO_2 flux measurement uncertainty inferred
761 from model residuals. Agric. For. Meteor., 148, 38-50, 2008.

762 Richardson, A.D., Williams, M., Hollinger, D.Y., Moore, D.J.P., Dail, D.B., Davidson,
763 E.A., Scott, N.A., Evans, R.S., Hughes, H., Lee, J.H., Rodrigues, C., Savage, K.:
764 Estimating parameters of a forest ecosystem C model with measurements of
765 stocks and fluxes as joint constraints. Oecologia, 164, 25-40, 2010.
766 Rutter, A.J., Kershaw, K. A., Robbins, P.C., Morton, A. J.: A predictive model of
767 rainfall interception in forests. I. Derivation of the model from observations in a
768 plantation of Corsican pine. Agric. For. Meteor., 9, 367-384, 1971.
769 Samanta, S., Mackay, D.S., Clayton, M.K., Kruger, E.L., Ewers, B.E.: Bayesian
770 analysis for uncertainty estimation of a canopy transpiration model. Water
771 Resour. Res., 43, W04424. http://dx.doi.org/10.1029/2006WR005028, 2007.
772 Sauer, T.J., Singer J.W., Prueger, J.H., DeSutter, T.M., Hatfield, J.L.: Radiation
773 balance and evaporation partitioning in a narrow-row soybean canopy. Agric. For.
774 Meteor., 145, 206-214, 2007.
775 Scott, R.L., Huxman, T.E., Cable, W.L., Emmerich, W.E.: Partitioning of
776 evapotranspiration and its relation to carbon dioxide exchange in a Chihuahuan
777 desert shrubland. Hydrol. Processes., 20, 3227-3243, 2006.
778 Sellers, P.J., Heiser, M.D., Hall, F.G.: Relations between surface conductance and
779 spectral vegetation indices at intermediate (100 m^2 to 15 km^2) length scales. J.
780 Geophys. Res., 97 (D17), 19033-19059, 1992.
781 Shuttleworth, W.J., Gurney, R.J.: The theoretical relationship between foliage
782 temperature and canopy resistance in sparse crops. Q. J. Roy. Meteor. Soc., 116,
783 497-519, 1990.

784 Shuttleworth, W.J., Wallace, J.S.: Evaporation from sparse crops- an energy
785 combination theory. Q. J. Roy. Meteor. Soc., 111, 839-855, 1985.
786 Stannard, D.I.: Comparison of Penman-Monteith, Shuttleworth-Wallace and modified
787 Priestley-Taylor evapotranspiration models for wildland vegetation in semiarid
788 rangeland. Water Resour. Res., 29, 1379-1392, 1993.
789 Stewart, J.B.: Modelling surface conductance of pine forest. Agric. For. Meteor., 43,
790 19-35, 1988.
791 Sun, H.Y., Shao, L.W., Liu, X.W., Miao, W.F., Chen, S.Y., Zhang, X.Y.:
792 Determination of water consumption and the water-saving potential of three
793 mulching methods in a jujube orchard. Eur. J. Agron., 43, 87-95, 2012.
794 Sun, S.F.: Moisture and heat transport in a soil layer forced by atmospheric conditions.
795 M.S. thesis, University of Connecticut, 1982.
796 Svensson, M., Jansson, P.E., Gustafson, D., Kleja, D.B., Langvall O., Lindroth, A.:
797 Bayesian calibration of a model describing carbon, water and heat fluxes for a
798 Swedish boreal forest stand. Ecol. Model., 213, 331-344, 2008..
799 Teh, C.B.S., Simmonds, L.P., Wheeler, T.R.: Modelling the partitioning of solar
800 radiation capture and evapotranspiration intercropping systems. In: Proceedings
801 of the 2nd International Conference on Tropical Climatology, Meteorology and
802 Hydrology TCMH-2001, Brussels, Belgium, 2001.
803 Tourula, T., Heikinheimo, M.: Modelling evapotranspiration from a barley field over
804 the growing season. Agric. For. Meteor., 91(3-4), 237-250, 1998.
805 United Nations Environment Programme (UNEP): World Atlas of Desertification.

806 London. Edward Arnold, 1992.
807 van de Griend, A.A., Owe, M.: Bare soil surface resistance to evaporation by vapor
808 diffusion under semiarid conditions. Water Resour. Res., 30 (2), 181-188, 1994.
809 van Oijen, M., Cameron, D.R., Butterbach-Bahl, K., Farahbakhshazad, N., Jansson,
810 P.E., Kiese, R., Rahn, K.H., Werner, C., Yeluripati, J.B.: A Bayesian framework
811 for model calibration, comparison and analysis: application to four models for the
812 biogeochemistry of a Norway spruce forest. Agric. For. Meteor., 151(12),
813 1609-1621, 2011.
814 van Oijen, M., Reyer, C., Bohn, F.J., Cameron, D.R., Deckmyn, G., Flechsig, M.,
815 Härkönen, S., Hartig, F., Huth, A., Kiviste, A., Lasch, P., Mäkelä, A., Mette, T.,
816 Minunno, F., Rammer, W.: Bayesian calibration, comparison and averaging of
817 six forest models, using data from Scots pine stands across Europe. Forest Ecol.
818 Manag., 289, 255-268, 2013.
819 van Oijen, M., Rougier, J., Smith, R.: Bayesian calibration of process-based forest
820 models: bridging the gap between models and data. Tree Physiol., 25(7), 915-927,
821 2005.
822 Verhoef, A., Allen, S.J.: A SVAT scheme describing energy and CO_2 fluxes for
823 multi-component vegetation: calibration and test for a Sahelian savannah. Ecol.
824 Model., 127, 245–267, 2000.
825 Verhoef, A., Fernández-Gálvez, J., Diaz-Espejo, A., Main, B.E., El-Bishti, M. The
826 diurnal course of soil moisture as measured by various dielectric sensors: effects
827 of soil temperature and the implications for evaporation estimates. J. Hydrol., 321,

147-162, 2006.

Verhoef, A., Ottle, C., Cappelaere, B., Murray, T., Saux-Picart, S., Zribi, M., Maignan, F., Boulain, N., Demarty, J., Ramier, D.: Spatio-temporal surface soil heat flux estimates from satellite data: results for the AMMA experiment at the Fakara (Niger) supersite. Agric. For. Meteor., 154-155, 55-66, 2012.

Villagarc á, L., Were, A., Garc á, M., Domingo, F.: Sensitivity of a clumped model of evapotranspiration to surface resistance parameterisations: Application in a semi-arid environment. Agric. For. Meteor., 150, 1065-1078, 2010.

Wallace, J.S., Verhoef, A.: Interactions in mixed-plant communities: light, water and carbon dioxide. In: Marshall B, Roberts JA (eds) Leaf development and canopy growth. Sheffield biological science series. Sheffield Academic Press, Sheffield, 204-250 pp., 2000.

Wang, J.M., Mitsuta, Y.: Evaporation from the desert: some preliminary results of HEIFI. Boundary-Layer Meteorol., 59, 413-418, 1992.

Wang, J.M., Zhuang, J.X., Wang, W.Z., Liu, S.M., Xu, Z.W.: Assessment of Uncertainties in Eddy Covariance Flux Measurement Based on Intensive Flux Matrix of HiWATER-MUSOEXE. IEEE Geosciences and Remote Sensing Letters, 2014, (under review).

Wang, X.F., Yakir, D.: Using stable isotopes of water in evapotranspiration studies. Hydrol. Process., 14, 1407-1421, 2000.

Wang, Y.P., Leuning, R., Cleugh, H.A., Coppin, P.A.: Parameter estimation in surface exchange models using nonlinear inversion: how many parameters can we

850 estimate and which measurements are most useful? Glob. Chang. Biol., 7,
851 495-510, 2001.
852 Williams, D.G., Cable, W., Hultine, K., Hoedjes, J.C.B., Yepez, E.A., Simonneaux, V.,
853 Er-Raki, S., Boulet, G., de Bruin, H.A.R., Chehbouni, A., Hartogensis, O.K.,
854 Timouk, F.: Evapotranspiration components determined by stable isotope, sap
855 flow and eddy covariance techniques. Agric. For. Meteor., 125 (3-4), 241-258,
856 2004.
857 Winsemius, H.C., Savenije1, H.H.G., Gerrits1, A.M.J., Zapreeva, E.A., Klees, R.:
858 Comparison of two model approaches in the Zambezi river basin with regard to
859 model reliability and identifiability. Hydrol. Earth Syst. Sci., 10, 339-352, 2006.
860 Xu, Z.W., Liu, S.M., Li, X., Shi, S.J., Wang, J.M., Zhu, Z.L., Xu, T.R., Wang, W.Z.,
861 Ma, M.G.: Intercomparison of surface energy flux measurement systems used
862 during the HiWATER-USOEXE. J. Geophys. Res., 118, 13140-13157, 2014.
863 Zhang, B.Z., Kang, S.Z., Li, F.S., Zhang, L.: Comparison of three evapotranspiration
864 models to Bowen ratio-energy balance method for a vineyard in an arid desert
865 region of northwest China. Agric. For. Meteor., 148, 1629-1640, 2008.
866 Zhang, Q., Huang, R.H.: Water vapor exchange between soil and atmosphere over a
867 Gobi surface near an oasis in Summer. Journal of Applied Meteorology, 43(12):
868 1917-1928, 2004.
869 Zhang, X.: Improvement of a Soil-Atmosphere-Transfer Model for the Simulation
870 of Bare Soil Surface Energy Balances in Semiarid Areas. Asia-Pacific J. Atmos.
871 Sci., 48(1), 97-105, 2012.

Zhao, W.Z., Ji, X.B., Kang, E.S., Zhang, Z.H., Jin, B.W.: Evaluation of Penman-Monteith model applied to a maize field in the arid area of northwest China. Hydrol. Earth Syst. Sci., 14, 1353-1364, 2010.

Zhu, G.F., Li, X., Su, Y.H., Lu, L., Huang, C.L.: Seasonal fluctuations and temperature dependence in photosynthetic parameters and stomatal conductance at the leaf scale of *Populus euphratica Oliv.*. Tree Physiol., 31(2), 178-195, 2011.

Zhu, G.F., Li, Z.Z., Su, Y.H., Ma, J.Z., Zhang, Y.Y.: Hydrogeochemical and isotope evidence of groundwater evolution and recharge in Minqin Basin, Northwest China. J. Hydrol., 333, 239-251, 2007.

Zhu, G.F., Su, Y.H., Feng, Q.: The Hydrochemical Characteristics and Evolution of Groundwater and Surface Water in the Heihe River Basin, Northwest China. Hydrogeol. J., 16, 167-182, 2008.

Zhu, G.F., Su, Y.H., Li, X., Zhang, K., Li, C.B.: Estimating actual evapotranspiration from an alpine grassland on Qinghai-Tibetan plateau using a two-source model and parameter uncertainty analysis by Bayesian approach. J. Hydrol., 476, 42-51, 2013.

Figure Lists:

894 **Fig. 1** Experimental location and instrumentation setting at Daman (DM) superstation.

895 **Fig. 2** Schematic diagram of the S-W model. From right to left, r_s^c and r_a^c are bulk
896 resistances of canopy stomatal and boundary layer (s m^{-1}), respectively; r_a^s and r_a^a
897 aerodynamic resistances from soil to canopy and from canopy to reference height (s
898 m^{-1}), respectively; r_s^s soil surface resistance (s m^{-1}). λT transpiration from canopy
899 (W m^{-2}), λE evaporation from soil under plant (W m^{-2}), and λET total
900 evapotranspiration (W m^{-2}).

901 **Fig. 3** Seasonal variation in (**a**) net solar radiation (R_n ; MJ m^{-2} d^{-1}), (**b**) air
902 temperature (T_a ; ^oC), (**c**) vapor pressure deficit (D ; kPa), (**d**) wind speed (u ; m s^{-1}) at
903 the height of 3 m, (**e**) precipitation and irrigation (mm), soil water content (θ, m^3 m^{-3})
904 at 4, 10 20 and 40 cm depth, and (**f**) leaf are index (LAI; m^2 m^{-2}) during the study
905 period in the Daman Oasis.

906 **Fig. 4** Histograms of samples from the posterior distributions of the parameters. The
907 dashed vertical lines indicate median parameter values.

908 **Fig. 5** Relative uncertainty reductions in the length of 95% credible interval form
909 prior to posterior distribution.

910 **Fig. 6** Comparisons of responses of soil surface resistance (r_s^s s m^{-1}) to soil surface
911 water contents (θ ; %) .

912 **Fig. 7** (**a**) Plot of estimated evapotranspiration (λET ; W m^{-2}) against observed values.
913 The regressions is: $y = 0.84x + 0.18$ ($R^2 = 0.83$); (**b**) Plot of estimated daily soil
914 evaporation (E; mm d^{-1}) against measured data. The regressions is: $y = 1.01x + 0.01$
915 ($R^2 = 0.82$).

916 **Fig. 8** Seasonal variation in daily evapotranspiration (ET; mm d^{-1}) and soil
917 evaporation (E; mm day^{-1}) measured by the EC system and modeled by the S-W
918 model during the study period in Daman Oasis. Gap in the time series is caused either
919 by the absence of flux measurements or missing ancillary data.

920 **Fig. 9** Diurnal variations in net radiation flux (R_n ; W m^{-2}), sensible heat flux (H; W
921 m^{-2}), and modeled and measured evapotranspiration flux (λET ;W m^{-2}). (**a**)-(**c**)
922 represented conditions at which micro-scale advection occurred at 12:00, 15:00 and
923 17:00 Beijing Standard Time (BST) , respectively, (**d**) represented a rainy day, and
924 (**e**)-(**h**) represented clear and advection-absent days during the study period. Gap is
925 caused either by the absence of flux measurements or missing ancillary data. Modeled
926 λET was presented as median $\pm 95\%$ posterior predication intervals.

927 **Fig. 10** The diurnal evolutions of temperature (T_a; ^oC) and relative humidity (RH; %)
928 profiles from 3 m to 40 m above the ground. (**a**) on 5 Jul. 2013. An obvious advection
929 process can be detected from 13:00 to 17:00 BST with high temperature and low RH
930 layer at the height of 8-18 m; (**b**) on 17 Jun. 2013. A precipitation event occurred at
931 13:00 and resulted in uniform vertical distributions of T_a and RH, but no temperature
932 inversion were observed; (**c**) on 11 Jun. 2013. It represented a typical clear and
933 advection-absent day.

934 **Fig. 11** Histograms depicting the frequency distribution of the
935 model-minus-observation departures for (**a**) half-hourly λET (W m^{-2}) and (**b**) daily
936 soil evaporation E (mm day^{-1}).

Table 1 Prior distributions and the parameter bounds for the S-W model. These values are derived from the literature; The posterior parameter distribution estimated by MCMC are based on observed data in our site, and are characterized by the mean and 95% high-probability intervals (Lower limit, Upper limit).

Parameter	Prior Distribution			Posterior Distribution	
	Lower Bound	Upper Bound	References	Median	95% High-Probability Interval
r_{STmin} (s m^{-1})	0	80	Noilhan and Planton (1989); Li et al. (2013a)	**21.8**	(20.2, 24.6)
k_1 (W m^{-2})	0	500	Stewart (1998)	294.6	(42.5, 487.7)
k_2 (^oC)	5	40	Ogink-Hendriks (1995)	**25.6**	(12.9,34.4)
k_3 (kPa^{-1})	0	0.1	Stewart (1998)	0.02	(0, 0.07)
b_1 (s m^{-1})	4	15	Sellers et al. (1992); Zhang (2012); Zhu et al., (2013)	**9.3**	(8.4, 10.0)
b_2 (s m^{-1})	0	8	Sellers et al. (1992); Zhang (2012) ; Zhu et al., (2013)	**6.2**	(3.8, 7.4)

The bold number means that this parameter was well constrained by the data.

Table 2 Statistical analysis of measured and estimated using the median parameter values half-hourly evapotranspiration (λET; W m^{-2}), daily soil evaporation (*E*; mm d^{-1}), and daily evapotranspiration(ET; mm d^{-1}) for the spring maize in arid desert oasis during the study period.

	n	Regressive equation	R^2	Mean measured values	Mean simulated values	RMSE	MBE	IA	EF
λET (W m^{-2})	3578	$\lambda ET_{modeled}=0.84\lambda ET_{measured}+0.18$	0.83	161.4	137.2	80.7	24.2	0.93	0.74
E (mm d^{-1})	56	$E_{modeled}=1.01E_{measured}+0.01$	0.82	0.26	0.28	0.05	-0.01	0.94	0.76
ET (mm d^{-1})	95	$ET_{modeled}=0.83ET_{measured}+0.19$	0.83	2.02	1.88	0.32	0.14	0.94	0.79

n=the sample number; R^2=the determination coefficient; RMSE=root mean square error; MBE=mean bias error between measured and modeled values; IA= index of agreement; ET= model efficiency. These statistical parameters are calculated using formulas given by Legates and McCabe (1999) and Poblete-Echeverria and Ortega-Farias (2009).

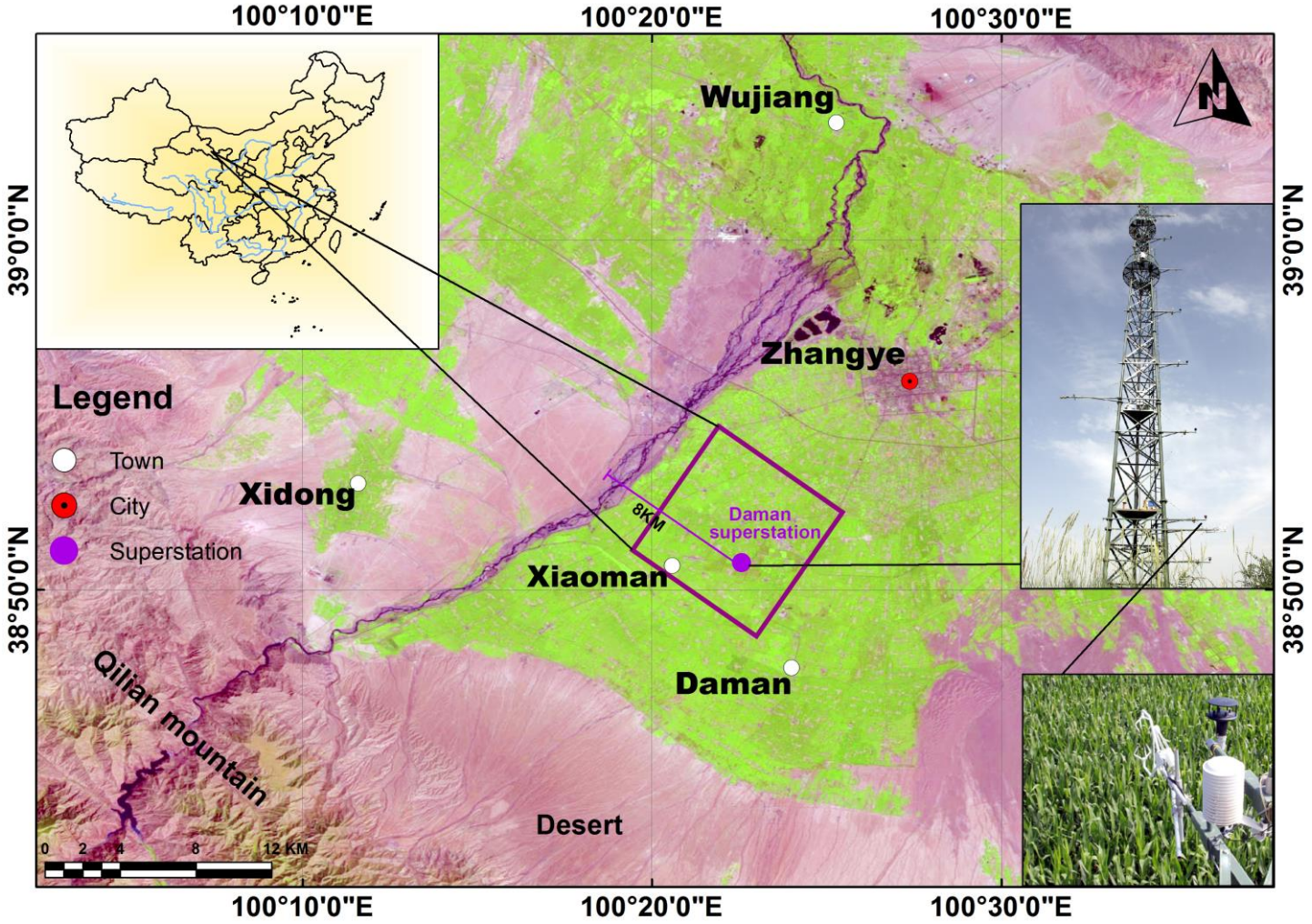
100°10'0"E
100°20'0"E
100°30'0"E
39°0'0"N
38°50'0"N
Wujiang
Zhangye
Xidong
Xiaoman
Daman
Daman superstation
8KM
Qilian mountain
Desert
Legend
Town
City
Superstation
0 2 4 8 12 KM
N

962

963 Fig. 1

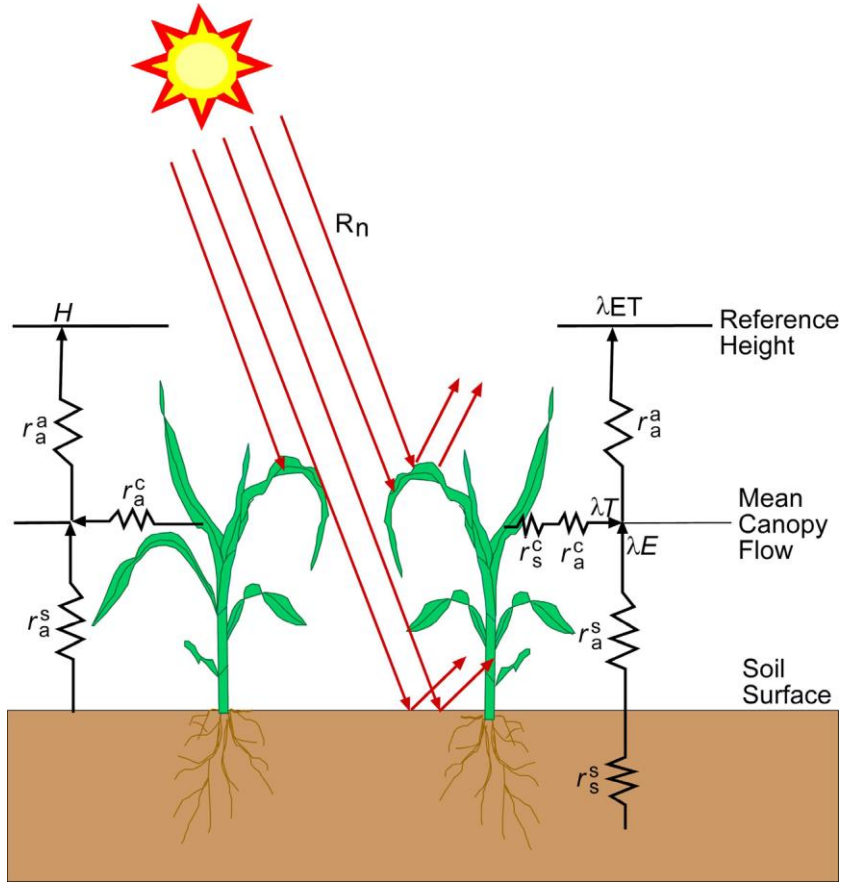

964

965 Fig. 2

966

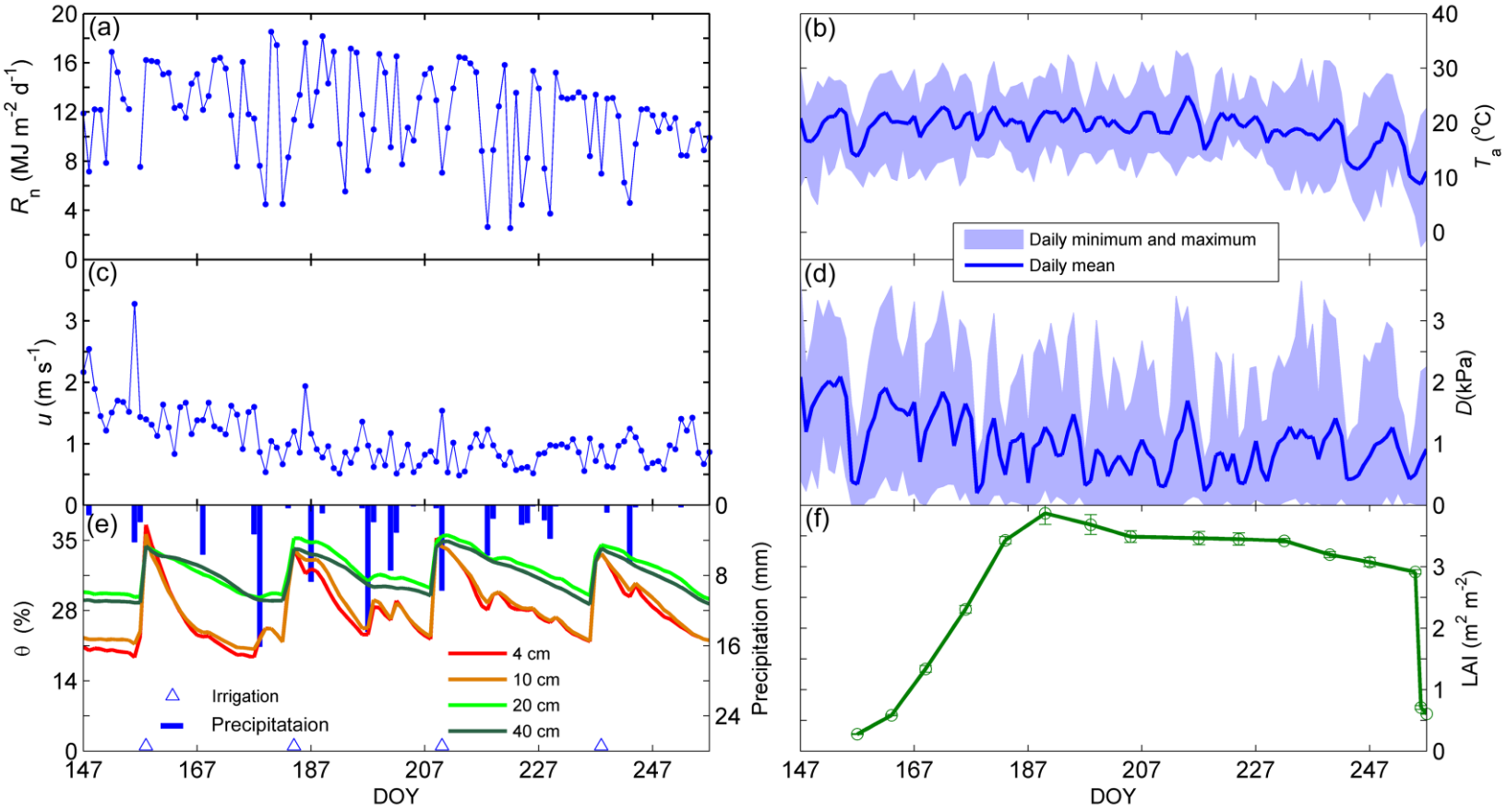
(a)
(b)
(c)
(d)
(e)
(f)
R_n (MJ m^{-2} d^{-1})
T_a (°C)
u (m s^{-1})
D(kPa)
θ (%)
Precipitation (mm)
LAI (m^2 m^{-2})
Daily minimum and maximum
Daily mean
Irrigation
Precipitataion
4 cm
10 cm
20 cm
40 cm
DOY
DOY

Fig. 3

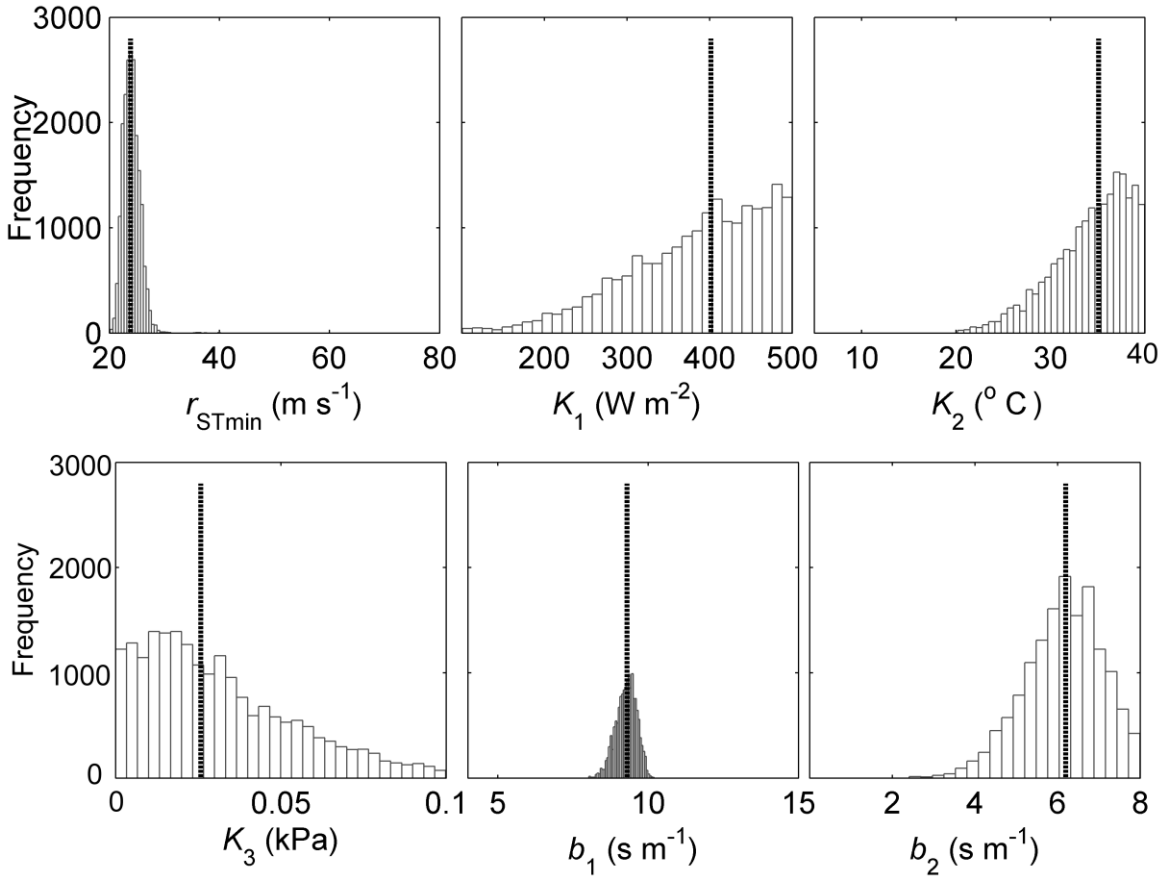
Frequency
3000
2000
1000
0
20
40
60
80
r_{STmin} (m s^{-1})
200
300
400
500
K_1 (W m^{-2})
10
20
30
40
K_2 (^{o} C)
0
0.05
0.1
K_3 (kPa)
5
10
15
b_1 (s m^{-1})
2
4
6
8
b_2 (s m^{-1})

Fig. 4

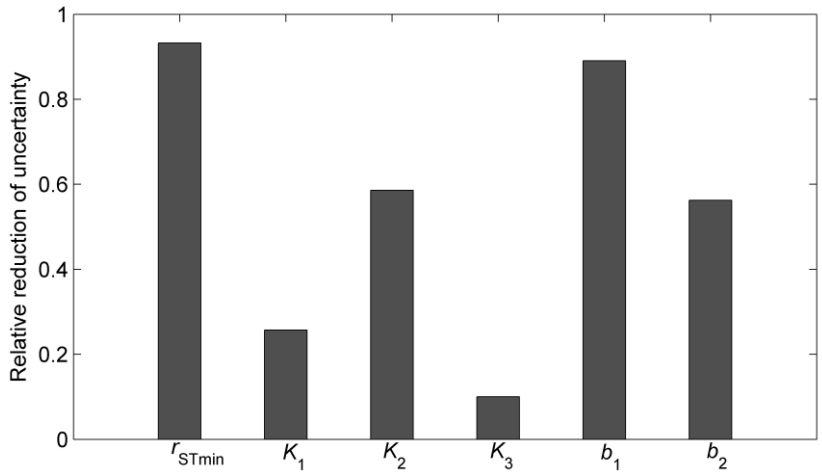
Relative reduction of uncertainty
1
0.8
0.6
0.4
0.2
0
r_{STmin}
K_1
K_2
K_3
b_1
b_2

Fig. 5

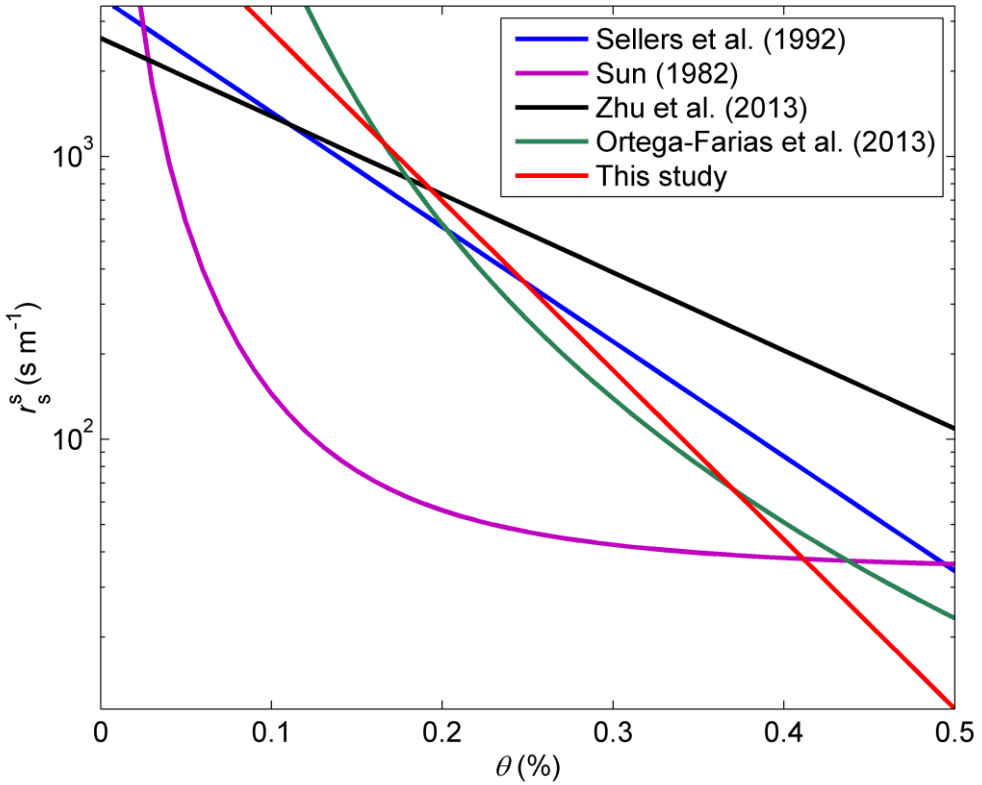
Sellers et al. (1992)
Sun (1982)
Zhu et al. (2013)
Ortega-Farias et al. (2013)
This study
10^3
10^2
r_s^s (s m^{-1})
0
0.1
0.2
0.3
0.4
0.5
θ (%)

Fig. 6

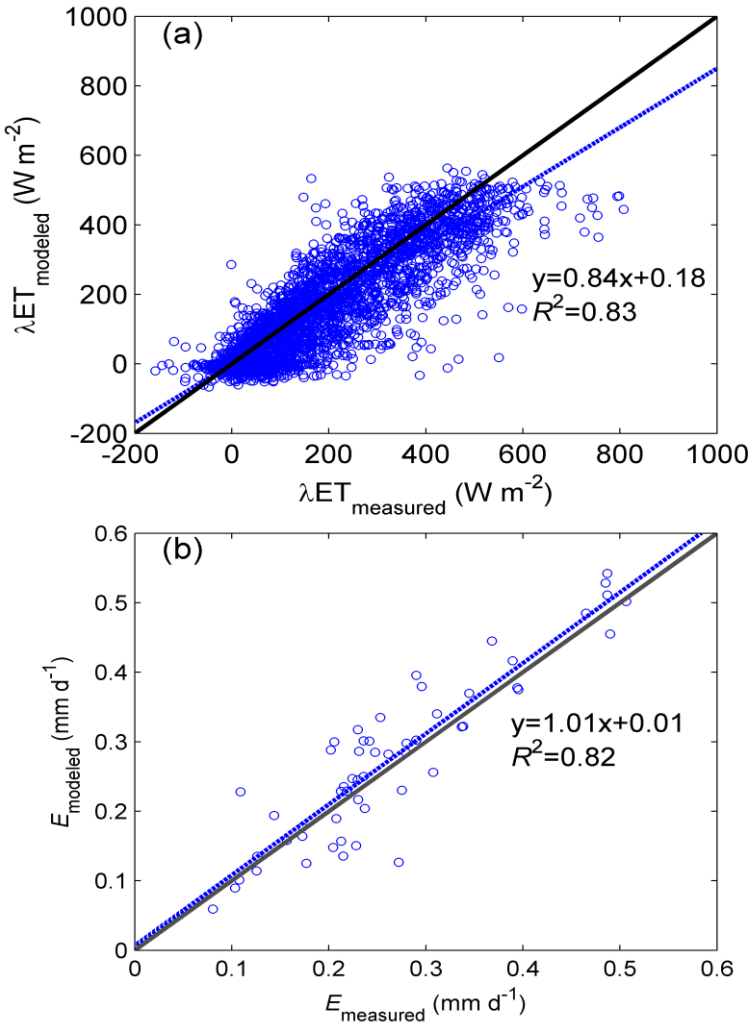
(a)
λET modeled (W m-2)
λET measured (W m-2)
y=0.84x+0.18
R2=0.83
(b)
E modeled (mm d-1)
E measured (mm d-1)
y=1.01x+0.01
R2=0.82

985

986 Fig. 7

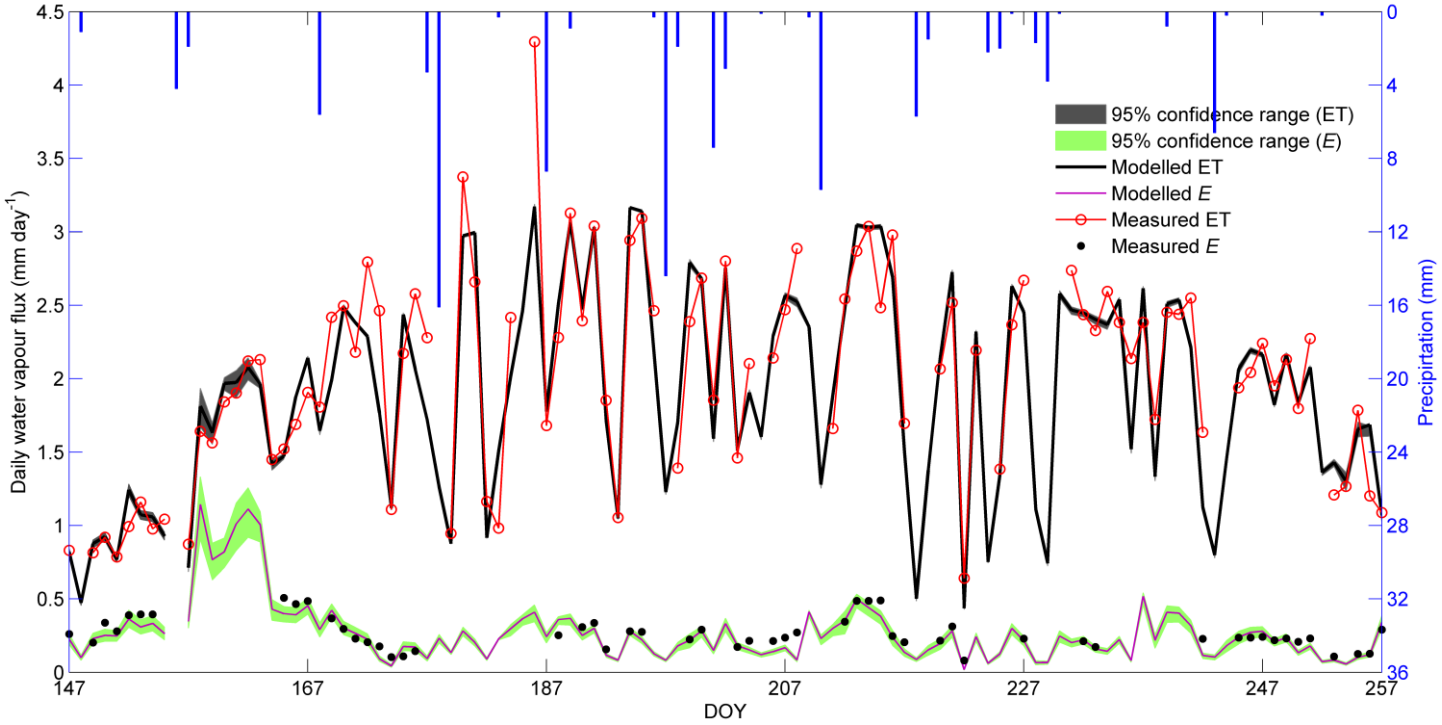
Daily water vapour flux (mm day-1)
Precipitation (mm)
DOY
95% confidence range (ET)
95% confidence range (E)
Modelled ET
Modelled E
Measured ET
Measured E
4.5
4
3.5
3
2.5
2
1.5
1
0.5
0
0
4
8
12
16
20
24
28
32
36
147
167
187
207
227
247
257

Fig. 8

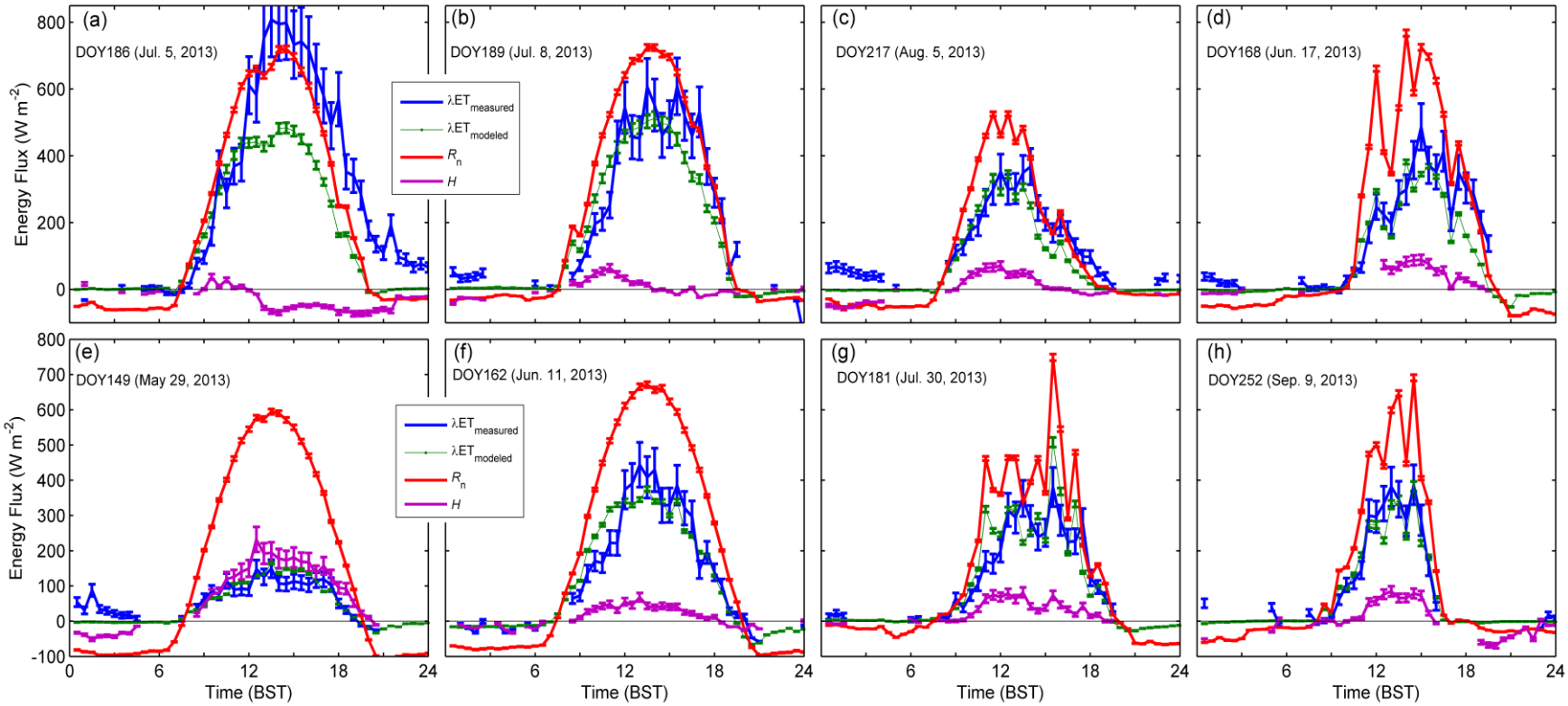
(a)
DOY186 (Jul. 5, 2013)
(b)
DOY189 (Jul. 8, 2013)
(c)
DOY217 (Aug. 5, 2013)
(d)
DOY168 (Jun. 17, 2013)
(e)
DOY149 (May 29, 2013)
(f)
DOY162 (Jun. 11, 2013)
(g)
DOY181 (Jul. 30, 2013)
(h)
DOY252 (Sep. 9, 2013)
λET measured
λET modeled
Rn
H
Energy Flux (W m-2)
Time (BST)

Fig. 9

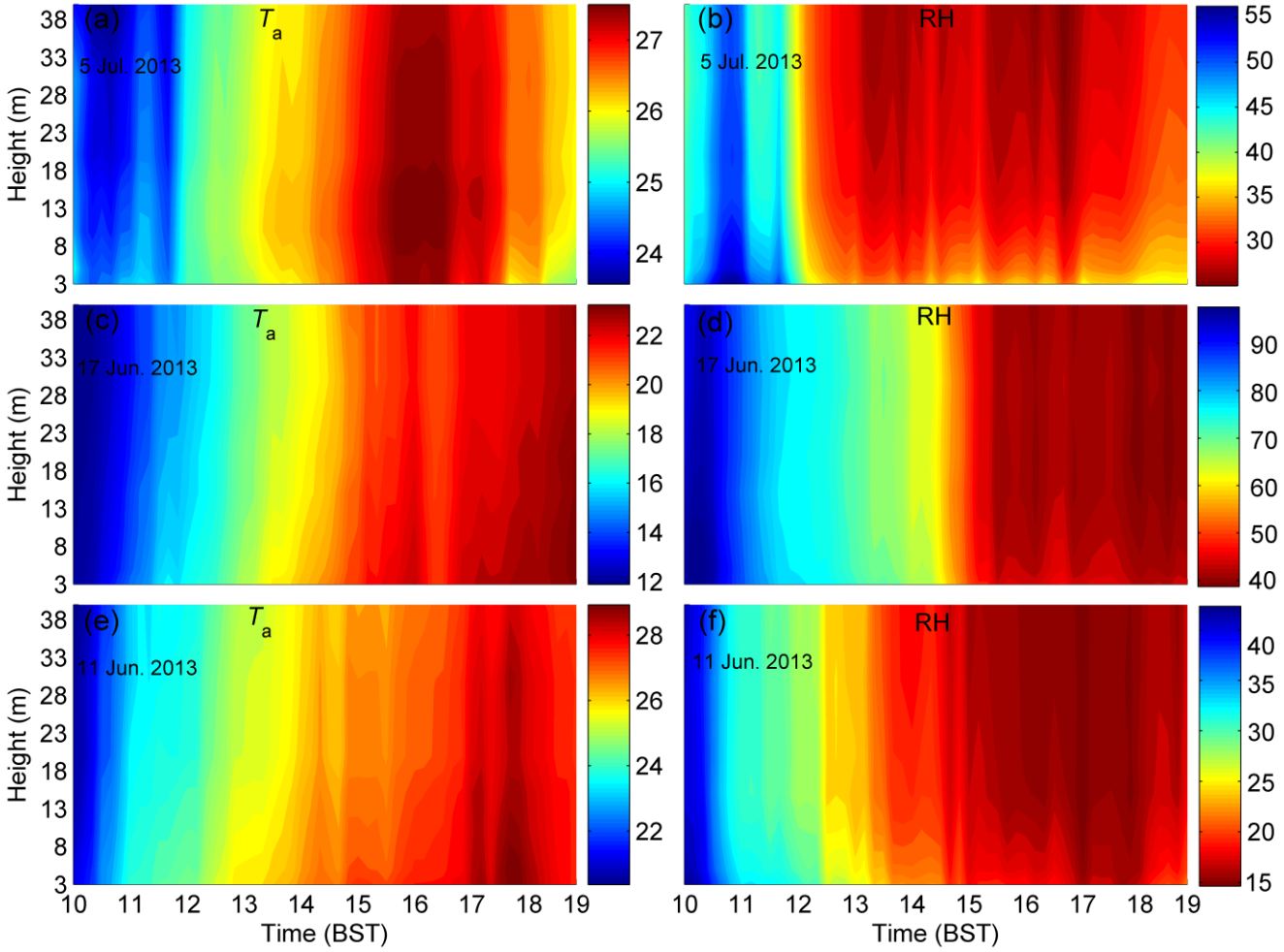

996

997 Fig. 10

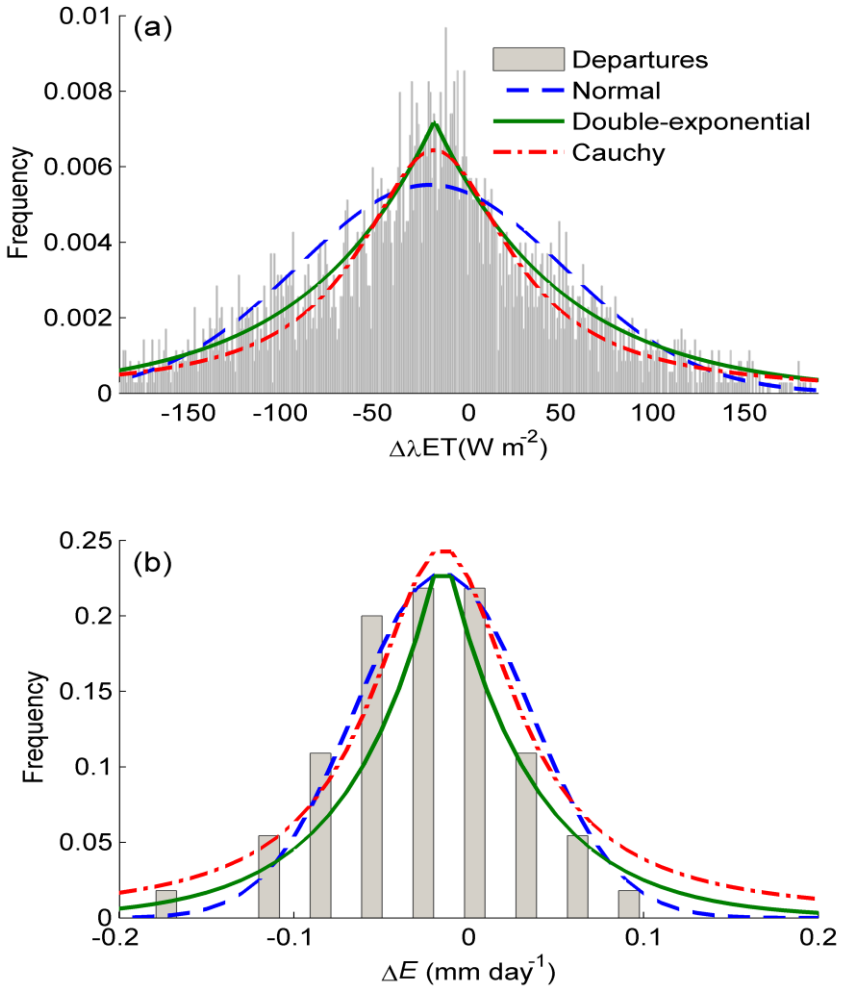

998

999 Fig. 11